ACS MATERIALS Au
AN OPEN ACCESS JOURNAL OF THE AMERICAN CHEMICAL SOCIETY

pubs.acs.org/materialsau

Review

Antiperovskite Superionic Conductors: A Critical Review

Jingfeng Zheng, Brian Perry, and Yiying Wu*

Cite This: *ACS Mater. Au* 2021, 1, 92–106

Read Online

ACCESS | Metrics & More | Article Recommendations

ABSTRACT: Antiperovskites of composition M_3AB (M = Li, Na, K; A = O; B = Cl, Br, I, NO_2, etc.) have recently been investigated as solid-state electrolytes for all-solid-state batteries. Inspired by the impressive ionic conductivities of $Li_3OCl_{0.5}Br_{0.5}$ and Na_3OBH_4 as high as 10^{-3} S/cm at room temperature, many variants of antiperovskite-based Li-ion and Na-ion conductors have been reported, and K-ion antiperovskites are emerging. These materials exhibit low melting points and thus have the advantages of easy processing into films and intimate contacts with electrodes. However, there are also issues in interpreting the stellar materials and reproducing their high ionic conductivities. Therefore, we think a critical review can be useful for summarizing the current results, pointing out the potential issues, and discussing best practices for future research. In this critical review, we first overview the reported compositions, structural stabilities, and ionic conductivities of antiperovskites. We then discuss the different conduction mechanisms that have been proposed, including the partial melting of cations and the paddlewheel mechanism for cluster anions. We close by reviewing the use of antiperovskites in batteries and suggest some practices for the community to consider.

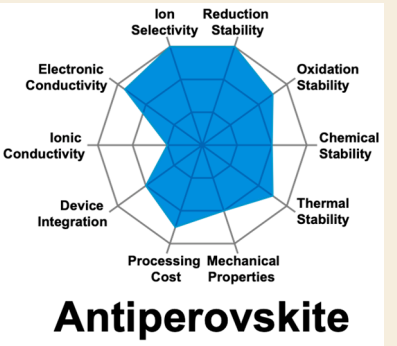

KEYWORDS: *solid-state electrolytes, antiperovskites, solid-state batteries, ion conduction mechanism, paddlewheel effect, partial melting*

1. INTRODUCTION

Recently, antiperovskite electrolytes have attracted attention for their applications in solid-state batteries as several high ionic conductivities have been reported. Specifically, in 2012, Zhao and Daemen reported a room temperature conductivity of 1.94×10^{-3} S cm^{-1} for $Li_3OCl_{0.5}Br_{0.5}$.[1] Braga et al. developed glassy $Li_{3-2x}Ba_xOCl$ (x = 0.005) with a conductivity of 2.5×10^{-2} S cm^{-1} at room temperature in 2014.[2] In 2019, Sun et al. reported Na_3OBH_4 reached 4.4×10^{-3} S cm^{-1} at room temperature after hot-pressing at 100 °C, outperforming other Na_3OX (X = Cl, Br) antiperovskites by several orders of magnitude.[3] However, attempts to reproduce these results have had mixed success and have complicated the situation. Moreover, the ion conduction mechanism in antiperovskite electrolytes is still under debate as several vacancy mechanisms and "paddlewheel" mechanisms have been suggested. Given the ongoing nature of these debates, we think a critical review of antiperovskite electrolytes is necessary to summarize the existing knowledge.

In this review, we first detail the crystal structures and chemical compositions of antiperovskites. Then the reported ionic conductivities are discussed, and points of confusion are specified. The different proposed ion conduction mechanisms are then summarized and compared. We also review the battery performance of tested antiperovskite materials, including their use as electrolytes and lithium reservoirs/cathodes, before concluding with a few suggestions on potential standard practices that may streamline future research efforts.

2. CRYSTAL STRUCTURES AND COMPOSITIONS OF ANTIPEROVSKITES

Before discussing the ionic conductivity reports, we will detail the crystal structure of antiperovskites. Antiperovskites have the same space group and crystal system as conventional perovskites (i.e., $Pm\bar{3}m$ and cubic) but with inverted cation−anion sites. The reported experimental antiperovskite crystal structures are summarized in Table 1 and Figure 1. The basic three-dimensional antiperovskite such as Na_3OBr has the composition M_3AB, where M is a cation, A is a divalent anion such as O^{2-}, and B is a monovalent anion such as a halide. They form corner-sharing M_6A octahedra, with the monovalent anion occupying the space between the octahedra. In addition to the three-dimensional cubic structure of antiperovskites, two-dimensional Ruddlesden−Popper (RP) phase antiperovskites such as Na_4OBr_2 also exist from the intergrowth of antiperovskite-layer and rocksalt-layer structures. Moreover, divalent O^{2-} in the A site can be replaced by monovalent OH^- or even neutral H_2O. To maintain charge neutrality, the M site has 1/3 and 2/3 vacancies. Moving a monovalent anion such as F^- or H^- to the A

Received: July 14, 2021
Revised: September 13, 2021
Accepted: September 14, 2021
Published: September 30, 2021

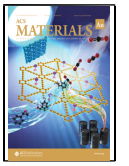

https://doi.org/10.1021/acsmaterialsau.1c00026
ACS Mater. Au 2021, 1, 92–106

Table 1. Summary of Reported Crystal Structures for Li and Na Antiperovskite Materials[a]

B	M	A	composition	space group	tolerance factor
O	Li	Cl	Li_3OCl[1]	$Pm\bar{3}m$	0.84
		Br	Li_3OBr[1]	$Pm\bar{3}m$	0.92
			$Li_7O_2Br_3$[11]	$I4/mmm$	
	Na	Cl	Na_3OCl[12]	$Pm\bar{3}m$	0.83
		Br	Na_3OBr[12]	$Pm\bar{3}m$	0.89
			Na_4OBr_2[13]	$I4/mmm$	
		I	Na_3OI[14]	$Pm\bar{3}m$	0.96
			Na_4OI_2[14]	$I4/mmm$	
		NO_2	Na_3ONO_2[15]	$Pm\bar{3}m$	0.89
			$Na_4O(NO_2)_2$[16]	$I4/mmm$	
		BH_4	Na_3OBH_4[3]	$Pm\bar{3}m$	0.94
		CN	Na_3OCN[15]	$Pm\bar{3}m$	0.89
			$Na_3O(CN)_2$[17]	$I4/mmm$	
OH	Li	Cl	Li_2OHCl[18]	$Pmc2_1$ (RT) to $Pm\bar{3}m$ (above 60 °C)	0.75
		Br	Li_2OHBr[19]	$Pm\bar{3}m$	0.82
			$Li_4(OH)_3Br$[20]	$P2_1/m$	
			$Li_5(OH)_2Br_3$[21]	$I4/mmm$	
H_2O	Li	Cl	$Li(H_2O)Cl$[22]	$Cmcm$	
		Br	$Li(H_2O)Br$[23]	$Pm\bar{3}m$	
F	Na	SO_4	Na_3FSO_4[5]	$P2_1/m$ (RT) to $R\bar{3}m$ (above 113 °C)	0.98
H	Li	S	LiHS[6]	$Pm\bar{3}m$	0.85
		Se	LiHSe[6]	$Pm\bar{3}m$	0.89
		Te	LiHTe[6]	$Pm\bar{3}m$	0.96
	Na	Se	NaHSe[6]	$Pnma$	0.80
		Te	NaHTe[6]	$Pm\bar{3}m$	0.87

[a]The ionic radii are based on refs 9 and 10.

site and placing a divalent anion like S^{2-} in the B site has also been reported.

The Goldschmidt's tolerance factor, t, is a frequently used criterion for the stability of perovskite structures.[4] It is based on a basic geometrical analysis of the component atoms' ionic radii. For the general formula M_3AB, it can be written as

$$t = \frac{r_A + r_M}{\sqrt{2}(r_B + r_M)}$$

where r_i is the ionic radius of atom i. A value of $t = 1$ indicates the ideal situation that three spherical ions fit perfectly in a cube. Size mismatch between the ions and phase instability exists when t deviates from unity. It may lead to distortions such as octahedral tilting. The tolerance factor of all reported antiperovskites is also included in Table 1. The results show that when $0.8 < t < 0.98$, the cubic structure exits. When t is too large, $[BM_{6/2}]$ octahedra may share faces to provide more space for larger A. Na_3SO_4F ($t = 0.98$) is an example. The structure of Na_3SO_4F can be described as triplets of face-sharing $[FNa_{6/2}]$ octahedra further linked by sharing corners.[5] When t is too small, $[BM_{6/2}]$ octahedra may have tilting. Hydride-based antiperovskites M_3HA (M = Li, Na; A = S, Se, Te) adopt the cubic structure except orthorhombic Na_3HS ($t = 0.80$).[6] $[HNa_{6/2}]$ octahedra has a $a^+b^-b^-$ tilting to accommodates a smaller A.

The well-known fast ion conductor Ag_3SI also has an antiperovskite structure.[7] Unfortunately, synthesis of the analogous Li_3SI and Na_3SI has not been achieved yet. Lapidus et al. suggested that the phase transitions of the two starting reactants, Ag_2S and AgI, to structures having the same body-centered cubic anion packing facilitate the formation of Ag_3SI.[8] However, in Na_3SI and Li_3SI, the phase transitions of the two starting reactants do not occur below their melting points. This hinders the formation of the corresponding antiperovskite structure.

Different calculation results have predicted that Li_3OCl (Li_3OBr) is metastable relative to Li_2O and LiCl (LiBr).[24,25] This is consistent with the experimental results from various research groups that the synthesis of H-free Li_3OCl is extremely challenging because of its highly hygroscopic nature, reacting with water to form Li_2OHCl and or $Li_4(OH)_3Cl$.[26−28] This also raises the question of whether the original synthesis of "Li_3OCl" that uses LiOH reacting with LiCl really produced the claimed material.[1] In contrast, lithium halide hydroxides such as Li_2OHCl are more stable[29] and have been consistently synthesized.[26,27,30] Also, for the synthesis of Na_3OI, the pure Na_3OI phase is difficult to achieve because the byproduct Na_4OI_2 emerges.[12] Therefore, the stability of three-dimensional and corresponding two-dimensional antiperovskites must be considered.

3. REPORTED IONIC CONDUCTIVITIES OF KNOWN ANTIPEROVSKITES

We now begin discussing the reported ionic conductivities for antiperovskite materials, which are listed along with their activation energies in Table 2. The characterization methods used are also included in Table 2 to stress the inconsistent rigor

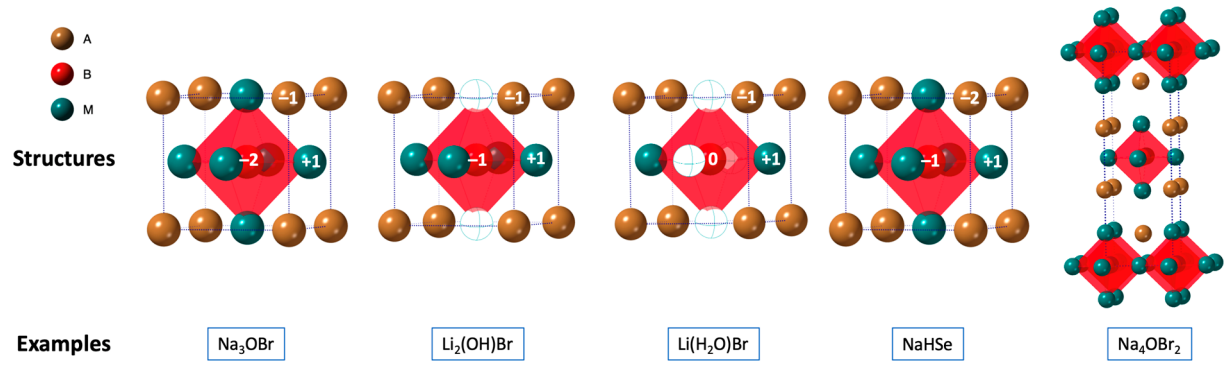

Figure 1. Possible crystal structures for antiperovskite materials.

https://doi.org/10.1021/acsmaterialsau.1c00026
ACS Mater. Au 2021, 1, 92−106

Table 2. Summary of Reported Ionic Conductivities and Activation Energies for Antiperovskite Materials[a]

material	research group	ionic conductivity (S cm^{-1}, temperature indicated)	activation energy (eV)	characterization	testing condition[b]
Li_2OHCl	Wang et al. 2020[44]	1.4×10^{-6} at 39 °C	0.55	refined PXRD, SXRD, NPD	ball-milled powder; hot-press (at 120 °C, 500 MPa); sputtered Au as electrode
Li_2OHCl	Song et al. 2018[18]	2×10^{-6} at 39 °C	0.54	refined PXRD, XPS, EDS, NMR	cold-press; Li or Au foils as electrodes
Li_2OHCl	Hartwig et al. 1981[19]	3×10^{-5} at 200 °C	0.97	not shown	melt solidify; Pt or Mo as electrodes (at 30−80 MPa)
Li_2OHCl	Koedtruad et al. 2020[36]	6.83×10^{-9} at RT	0.60 (cubic phase)	refined SXRD	cold-press; graphite as electrodes
		1.01×10^{-6} at 60 °C			
Li_2OHCl	Howard et al. 2017[45]	8×10^{-9} at RT	0.65 (cubic phase)	refined PXRD	cold-press (at 300 MPa); Al/C as electrodes
		3×10^{-7} at 60 °C			
$Li_{2.7}OH_{0.3}Cl$	Song et al. 2018[18]	7.6×10^{-8} at 40 °C	0.58	refined PXRD, XPS, EDS	cold-press; Li or Au foils as electrodes
$Li_{3-n}(OH_n)Cl$ ($0.83 \leq n \leq 2$)	Schwering et al. 2003[22]	4.2×10^{-5} at 60 °C ($n = 1$)	0.56 ($n = 1$)	unrefined PXRD, NMR, DSC	cold-press (at 350 MPa); Au as electrodes
		10^{-8} from 0 to 60 °C ($n = 2$)			
Li_2OHCl	Hood et al. 2016[30]	2×10^{-8} at RT, 1.2×10^{-5} at 60 °C	0.56	unrefined PXRD, SEM	ball-milled powder; cold-press (at 300 MPa); Al/C as electrodes
$Li_2(OH)_{0.9}F_{0.1}Cl$	Li et al. 2016[28]	3.5×10^{-5} at RT	0.52	unrefined PXRD with impurities, SEM	melt quench; Al or Li foil as electrodes
Li_3OCl	Zhao et al. 2012[1]	0.85×10^{-3} at RT	0.26	unrefined PXRD with impurities, DSC	keep in molten state for 100 h; molt quench on Al foil; cut crystalline bulk into disk-shaped sample; sputtered Au with Au foil as electrodes
$Li_3OCl_{0.5}Br_{0.5}$		1.94×10^{-3} at RT	0.18		
Li_3OCl	Lu et al. 2014[46]	5.8×10^{-7} at RT	0.59	unrefined XRD	cold-press (14 MPa); annealing (300 °C)
Li_3OCl film	Lu et al. 2014[46]	8.9×10^{-6} at RT	0.36	unrefined XRD	pulsed laser deposition film on Ag or Li using Li_3OCl target
$Li_5(OH)_2Cl_3$	Hood et al. 2016[30]	1.48×10^{-7} at RT	0.48	unrefined PXRD, SEM.	ball-milled powder; cold-press (at 300 MPa); Al/C as electrodes
Li_3OBr	Li et al. 2016[31]	1×10^{-6} at RT	0.74	unrefined PXRD, FT-IR, DSC	melt and pressed between Au foil
Li_3OBr	Zhu et al. 2016[11]	1×10^{-6} at RT	0.7	refined PXRD	melt between Au foil
$0.44Li_7O_2Br_3$; $0.56Li_3OBr$	Zhu et al. 2016[11]	2.4×10^{-5} at RT	0.4	refined PXRD	melt and pressed between Au foil
Li_2OHBr	Li et al. 2016[28]	1.3×10^{-6} at RT	0.75	unrefined PXRD	melt quench; Al or Li foil as electrodes
$Li_{3-n}(OH_n)Br$ ($1 \leq n \leq 2$)	Schwering et al. 2003[22]	1.2×10^{-7} at 50 °C ($n = 1$)	0.75 ($n = 1$)	unrefined PXRD, NMR, DSC.	cold-press (at 350 MPa); Au as electrodes
		1.3×10^{-6} at 50 °C ($n = 2$)	0.68 ($n = 2$)		
Li_2OHBr	Sugumar et al. 2020[35,47]	1.1×10^{-6} at RT	0.54	unrefined PXRD, FT-IR	ball-milled powder; cold-press (510 MPa for 5 min); Au as electrodes
$Li_2OHBr_{0.75}Cl_{0.25}$	Sugumar et al. 2021[35]	4.6×10^{-7} at RT	0.59	unrefined SXRD	
$Li_2OHBr_{0.9}I_{0.1}$	Sugumar et al. 2021[35]	4.9×10^{-6} at RT	0.41	unrefined SXRD	
Li_2OHBr	Koedtruad et al. 2020[36]	1.3×10^{-7} at 30 °C	0.56	refined SXRD	cold-press; no sintering; graphite as electrodes
Li_2OHBr	Song et al. 2018[18]	3.2×10^{-7} at 21 °C	0.59	refined PXRD, XPS, EDS	cold-press; Li or Au foils as electrodes
Li_2OHBr	Hartwig et al. 1981[19]	5×10^{-5} at 200 °C		not shown	melt solidify; no sintering; Pt or Mo as electrodes (at 30−80 MPa)
Li_2OHI		3×10^{-6} at 150 °C	1.24		
$LiOHBr_{0.98}F_{0.02}$	Yin et al. 2020[48]	1.1×10^{-6} at RT	0.62	unrefined PXRD, EDS, SEM, XPS	stainless steel as electrodes
Li_3OCl	Braga et al. 2014[2]	2.1×10^{-3} at RT	0.49	refined PXRD with impurities, DSC	stainless steel or Au as electrodes
Li_3HS	Gao et al. 2021[6]	9×10^{-10} at RT	0.50	refined SXRD, NPD	cold-press (at 18 MPa for 1 min); stainless steel rods as electrodes
Li_3HSe		2×10^{-9} at RT	0.52		
Li_3HTe		5×10^{-9} at RT	0.49		
Na_3HS		1×10^{-7} at RT	0.30		
Na_3HSe		7×10^{-8} at RT	0.53		
Na_3HTe		8.2×10^{-6} at RT	0.43		
Na_3OBr	Wang et al. 2015[12]	1.0×10^{-4} at 200 °C	0.76	refined PXRD refinement, DSC,	melt within Au foils (at 280 °C); anneal (at 230 °C)
Na_3OCl		3.0×10^{-5} at 200 °C	0.63		
$Na_3OBr_{0.6}I_{0.4}$		9.8×10^{-5} at 160 °C	0.63		

https://doi.org/10.1021/acsmaterialsau.1c00026
ACS Mater. Au 2021, 1, 92−106

Table 2. continued

material	research group	ionic conductivity (S cm^{-1}, temperature indicated)	activation energy (eV)	characterization	testing condition[b]
$Na_{2.9}Sr_{0.05}OBr_{0.6}I_{0.4}$		2.8×10^{-6} at RT, 1.9×10^{-3} at 200 °C	0.62		
Na_3OBr	Nguyen et al. 2016[39]	2.5×10^{-6} at 200 °C	0.84	refined PXRD, EDS, SEM	spark plasma sinter (at 450 °C, 60 MPa for 5 min); colloidal silver paste as electrodes
		1.7×10^{-7} at 200 °C	1.14		cold-press (at 60 MPa); sinter (at 450 °C for 24 h) and quench; colloidal silver paste as electrodes
$Na_3O(BH_4)$	Sun et al. 2019[3]	4.4×10^{-3} at RT	0.25	refined PXRD, NMR	cold-press (at 300 MPa); sinter (at 100 °C for 12 h with applied pressure); pressed Au powder as electrodes
$Na_3O(BH_4)$	Ahiavi et al. 2020[34]	3.8×10^{-9} at 40 °C	0.81	refined PXRD, TGA, DSC, FT-IR	cold-press (at 750 MPa); graphite paper disks as electrodes
Na_3OCl		1×10^{-10} at 40 °C	1.04		
Na_3OBr		4×10^{-9} at 40 °C	0.81		
$Na_3OCl_{0.5}Br_{0.5}$		4.7×10^{-10} at 40 °C	0.91		
$Na_3OBr_{0.5}(BH_4)_{0.5}$		8.8×10^{-10} at 55 °C	0.73		
Na_3OBr	Zhu et al. 2016[49]	1.3×10^{-8} at 30 °C	0.68	refined NPD	melt between Au foil electrodes
Na_4OI_2		1.6×10^{-8} at 30 °C	0.65		
Na_3ONO_2	Gao et al. 2020[50]	3.7×10^{-4} at 212 °C	0.39	refined PXRD, refined NPD, DSC	hot-press (at 300 MPa, 100 °C for 5 h); stainless steel rods as electrodes
Na_3ONO_2	Jansen et al. 1992[37,38]	1.26×10^{-4} at 230 °C	0.95	DSC	Ag foils as electrodes
Na_3OCN		7.59×10^{-3} at 237 °C	0.70		
Na_3OBr		7.61×10^{-5} at 227 °C	0.52		
$K_3(BH_4)(B_{12}H_{12})$	Sadikin et al. 2017[42]	2×10^{-6} at 107 °C		refined SXRD, DSC, NMR	cold-press; gold as electrodes
K_3OI	Zheng et al. 2021[43]	2.5×10^{-4} at 245 °C (high T phase)	1.30 (high T phase)	refined PXD, SXRD, DSC, Raman, SEM, EDS	cold-press; sinter (at 300 °C for 12 h); sputtered Pt as electrodes
$K_{2.9}Ba_{0.05}OI$		3.5×10^{-3} at 250 °C (high T phase)	0.36 (high T phase)		

[a]Characterization mentioned in the table: powder X-ray diffraction (PXRD), synchrotron X-ray powder diffraction (SXRD), neutron powder diffraction (NDP), X-ray photoelectron spectroscopy (XPS), nuclear magnetic resonance (NMR), differential scanning calorimetry (DSC), energy-dispersive spectroscopy (EDS), Fourier transform infrared spectroscopy (FT-IR), thermogravimetric analysis (TGA), scanning electron microscope (SEM), and Raman spectroscopy (Raman). [b]Pellet sample is used for ionic conductivity measurement without notion.

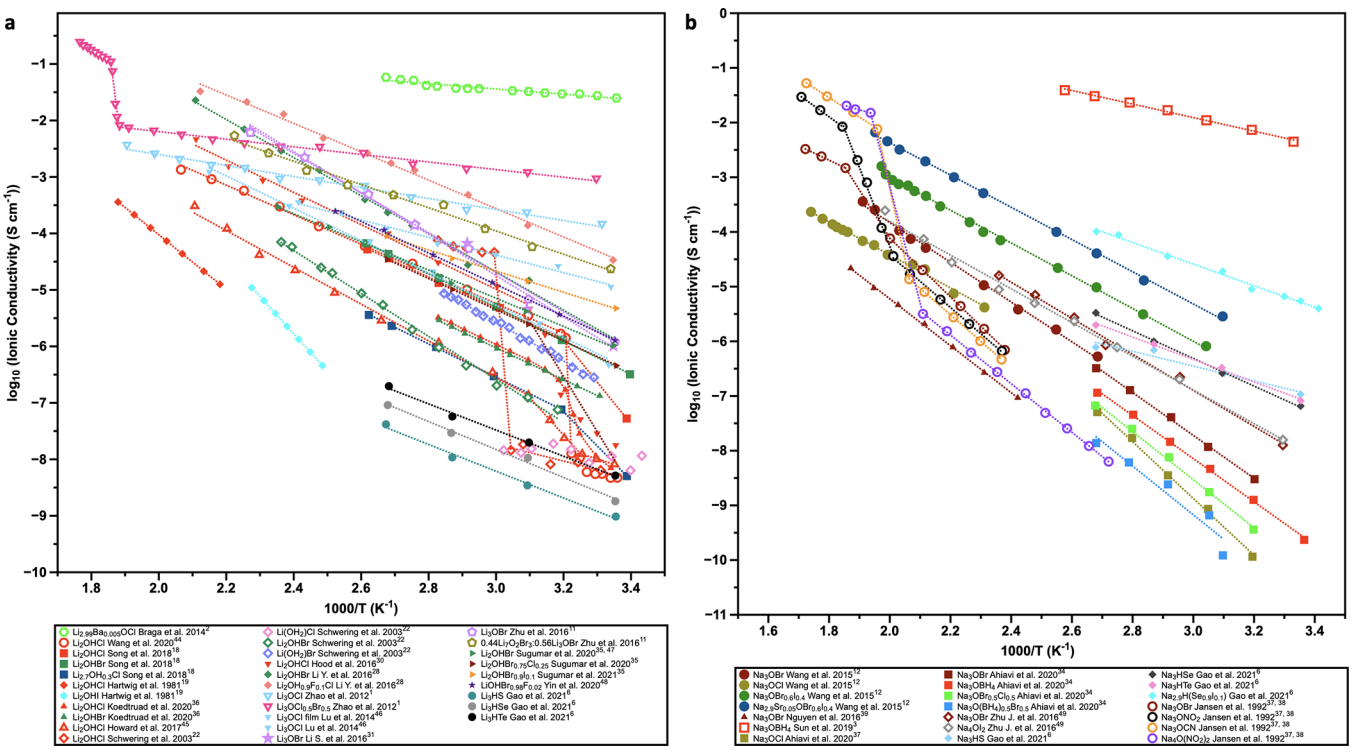

Figure 2. (a) Plot of reported Arrhenius plots for Li antiperovskites. (b) Plot of reported Arrhenius plots for Na antiperovskites. Dashed lines are only for visual guidance. Different chemical compositions are grouped by colors. Different literature references are grouped by markers.

https://doi.org/10.1021/acsmaterialsau.1c00026
ACS Mater. Au 2021, 1, 92−106

of research and facilitate our critical discussion. For ease, Arrhenius conductivity plots for Li-ion conductors and Na-ion conductors are shown in Figure 2a,b, respectively.

3.1. $Li_3OBr_{0.5}Cl_{0.5}$, Li_3OCl Glass, and Na_3OBH_4: The Three Stars under Question

In 2012, Zhao et al. reported Li_3OX (X = Cl or Br) with ionic conductivity higher than 10^{-3} S cm^{-1} at room temperature.[1] The sample was synthesized by heating molten LiX and LiOH as the starting materials under vacuum for several days: LiCl + 2LiOH = Li_3OCl + H_2O. The study claimed the chemical equilibrium was driven to the right and formed Li_3OCl by continuous heating under high vacuum. In addition, the sample preparation and measurement process have a significant impact on the final ionic conductivity of the sample. Annealing the sample in a vacuum above 250 °C for 24 h dramatically enhances the ionic conductivity by 2 orders of magnitude from the range of 10^{-7} S cm^{-1}. The highest reported ionic conductivity even achieves 1.94×10^{-3} S cm^{-1} for $Li_3OCl_{0.5}Br_{0.5}$. It is worth noting that no characterization was carried out to evaluate the possible structural change for the ionic conductivity boost. Later in 2016, Li et al. from the same group did follow-up research and systematically studied the reaction mechanism of Li_3OX synthesis.[31] Their theoretical calculation showed that Li_3OCl is not thermodynamic stable compared with Li_2O and LiCl.[24] They showed that ball milling of starting material followed by heating can produce a pure Li_3OBr sample. However, the ionic conductivity of synthesized Li_3OBr only shows bulk and grain boundary conductivity of 1.02×10^{-5} and 1.09×10^{-6} S cm^{-1}, respectively. They also suggested that the superionic Li_3OCl sample was synthesized by heating at 360 °C under vacuum for several days, which probably resulted from LiCl deficiency and produced $Li_{3-n}OX_{1-n}$ ($n > 0$). Al^{3+} may have been incorporated into the sample when the sample was melted between Al foil for ionic conductivity tests. Hence, the superionic behavior of Li_3OCl is still somewhat questionable.

In 2014, Braga et al. reported $Li_{3-2x}Ba_xOCl$ glass ($x = 0.005$) with extremely high ionic conductivity of 2.5×10^{-2} S cm^{-1} at 25 °C.[2] It must be noted that the reported synthesis is vague. The electrolyte was prepared by heating LiOH, LiCl, and $Ba(OH)_2$ with several drops of water in a Teflon reactor at 220−240 °C. Water was dried out by heating and then vacuum pumping to form the crystalline sample. The synthesized crystalline sample was heated in air to form the final glass sample. Hanghofer et al. carefully repeated the synthesis and found that the crystalline sample was indeed a mixture of $Li_{1.84}H_{1.16}OCl$ and $Li_4(OH)_3Cl$.[27] Moreover, after heating at the air, $Li_{1.84}H_{1.16}OCl$ and $Li_4(OH)_3Cl$ should form $LiCl{\cdot}xH_2O$, which has a very high electrical conductivity.[32,33]

In 2019, Sun et al. first synthesized Na_3OBH_4 from Na_2O and $NaBH_4$. The reported ionic conductivity is 4.4×10^{-3} S cm^{-1} at room temperature, which is several orders of magnitude higher than Na_3OX (X = Cl, Br, I) mentioned above (Table 2). The activation energy is only 0.25 eV. Sun et al. attributed the improvement to the cubic structure and the rotation of the BH_4^- clusters. Moreover, the impressive conductivity could only be achieved by hot-pressing at 100 °C, which lowered the resistance to below 20 Ω. The cold-pressed sample, on the contrary, gives resistance on the MΩ level. However, Ahiavi et al. repeated the synthesis of Na_3OBH_4 and achieved an ionic conductivity of only 10^{-10} S/cm, 7 orders of magnitude lower than what Sun et al. reported.[34] Ahiavi et al. argued that hot-pressing could not make such a significant difference in total resistance (from MΩ level to less than 20 Ω). In addition, Ahiavi et al.'s AIMD simulation results show that although BH_4^- anion rotates at all the temperature test (600−800 K), the computed Na^+ diffusivities for Na_3OBH_4 are still of the same order of magnitude as Na_3OX (X = Cl, Br, I). Hence, the superionic behavior of Na_3OBH_4 still needs further research to confirm.

3.2. Other Li-Ion Conductors

In 1981, Hartwig et al. first reported utilizing the quasi-binary system of LiOH−LiX (X = Cl, Br, and I) as a solid-state electrolyte.[19] For LiOH−LiCl, they stated the ionic conductivity for $Li_2(OH)Cl$ and $Li_5(OH)_3Cl_2$ at 200 °C is 3×10^{-5} and 7.5×10^{-4} S cm^{-1}, respectively. For LiOH−LiBr, the ionic conductivity of $Li_2(OH)Br$ is 5×10^{-5} S cm^{-1}; for LiOH−LiI, the ionic conductivity for $Li_2(OH)I$ and $Li_5(OH)_4I$ at 150 °C is 3×10^{-6} and 2×10^{-5} S cm^{-1}, respectively. The crystal structure was confirmed from powder X-ray diffraction (XRD) only for $Li_2(OH)Br$. In 2016, Hood et al. synthesized the binary phase of LiOH and LiCl with ratios of 1:2, 2:3, 1:1, 3:2, and 1:1. No Rietveld refinement was done to confirm the product purity. At room temperature, the fast-cooling sample $Li_5(OH)_2Cl_3$ (2:3 ratio) shows the highest ionic conductivity 1.48×10^{-7} S cm^{-1}. The cooling rate of synthesis has been shown to have an impact on the sample's ionic conductivity. At 100 °C, the fast-cooling electrolyte has approximately 1 order of magnitude ionic conductivity higher than the slow-cooling sample. Authors assigned this enhancement to the increase of defects in the lattices during fast cooling. However, in 2018, Hanghofer et al. argued that only $Li_2(OH)Cl$ and $Li_4(OH)_3Cl$ are only stable phases for LiOH and LiCl binary system.[27]

In 2003, Schwering et al. thoroughly studied the ionic conductivity and phase transition of $Li_{3-n}(OH_n)X$ ($0.83 \leq n \leq 2$; X = Cl, Br) using impedance measurement and ^1H and ^7Li NMR spectroscopy.[22] For $Li_{3-n}(OH_n)Cl$, $Li_2(OH)Cl$ transitions from orthorhombic to cubic symmetry at 35 °C with a 3 orders of magnitude increase in the ionic conductivity, which achieves 10^{-4} S cm^{-1} at 50 °C. The Li-doped $LiCl{\cdot}H_2O$−$Li_{1.16}(OH_{1.84})Cl$ stabilizes the high ionic conductivity cubic phase at room temperature. $LiCl{\cdot}H_2O$ with orthorhombic structure has a low ionic conductivity (10^{-8} S cm^{-1}) in the entire temperature range (0−60 °C). The study of $Li_{3-n}(OH_n)Br$ further confirms the trend that the cubic symmetry has a higher ionic conductivity and Li doping may help to stabilize the cubic symmetry. $LiBr{\cdot}H_2O$ transitions from orthorhombic to cubic symmetry at 33 °C with an increase of ionic conductivity. Li doping of $LiBr{\cdot}H_2O$ also helps to stabilize the cubic phase at room temperature. In addition, according to the temperature-dependent behavior on impedance test and NMR spectroscopy, the activation energy of grain conductivity and grain boundary conductivity is estimated to be in the range of 30−37 and 60−70 kJ mol^{-1}, respectively. Later, Song et al. studied the ionic conductivity of $Li_{3-n}(OH_n)Cl$ (n = 0.3, 0.6, 0.9, and 1) and $Li_2(OH)Br$.[18] Contradictory to what Schwering et al. state, $Li_{2.17}(OH_{0.83})Cl$ shows the conversion from tetragonal to cubic at −60 °C, and Song et al. claimed that all $Li_{3-n}(OH_n)Cl$ (n = 0.3, 0.6, 0.9, and 1) exist as orthorhombic phases at room temperature and converted to cubic phase upon heating. Moreover, both from experimental tests and MD simulation, $Li_{3-n}(OH_n)Cl$ show a decrease on the total ionic conductivity with decrease on the amount of proton. Those results indicate H facilitates Li diffusion through the paddlewheel effect, which will be discussed in more detail later.

https://doi.org/10.1021/acsmaterialsau.1c00026
ACS Mater. Au 2021, 1, 92−106

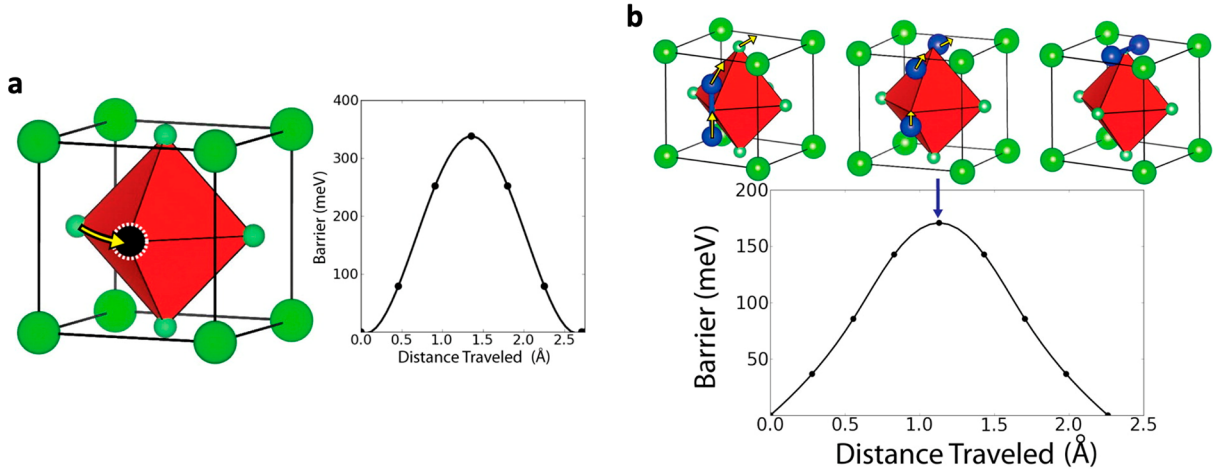

Figure 3. (a) Lithium migration into a vacant site (black with dotted white line). (b) Li ions migrate through Frenkel defects. Reproduced from ref 24. Copyright 2013 American Chemical Society.

In addition to Li doping, anion substitutions have been shown to affect the ionic conductivity. Sugumar et al. studied how anion mixing affects the ionic conductivity for $Li_2OHBr_{1-n}X_n$ (X = Cl, I).[35] They found that the mixing of I increases the lattice constant and also the ionic conductivity. On the contrary, the mixing of Cl decreases the lattice constant and the ionic conductivity. Li et al. used F^- to dope Li_2OHCl to form $Li_2(OH)_{1-n}F_nCl$.[28] Substitution of F^- for OH^- transforms the orthorhombic Li_2OHCl to cubic phase at room temperature, which is reported to have a higher ionic conductivity compared.[36] However, the XRD results still show some impurities, and it is hard to ensure that F^- substitutes the OH^- site and not the Cl^- site. According to the theoretical study of Effat et al., Li_2OHCl, $Li_2(OH)_{0.9}F_{0.1}Cl$, and $Li_2OHF_{0.1}Cl_{0.9}$ can all be synthesized to pure phases. Among them, $Li_2OHF_{0.1}Cl_{0.9}$ has the highest ionic concavity and lowest activation energy.[29]

For the choice of anions, Gao et al. showed antiperovskites can also be formed by hydride and chalcogenide anion to form a family of M_3HCh antiperovskites (M = Li, Na).[6] The M_3HCh antiperovskites adopt the ideal cubic structure except for orthorhombic Na_3HS. They claimed the low migration barriers are promoted by a soft phonon mode associated with the rotational motion of HM_6 octahedra in their cubic forms. Aliovalent substitution of chalcogenide to create cation vacancies has further enhanced ionic conductivities to achieve a conductivity of ~1 × 10^{-4} S cm^{-1} (100 °C) for $Na_{2.9}H(Se_{0.9}I_{0.1})$.

3.3. Antiperovskite Na-Ion Conductors

Unlike Li_3OX materials, the Na_3OX (X = Cl, Br, I, CN, NO_2) family is thermodynamically stable compared with the starting materials Na_2O and NaX. Consequently, antiperovskite Na-ion conductors have been a robust area of research. In 1991, Jansen studied the ionic conduction behavior of Na_3OX (X = Br, CN, NO_2), all three of which have one or two significant conductivity jumps near 500 K from 10^{-4} to 10^{-3}–10^{-2} S cm^{-1}.[37,38] As his work is integral to the paddlewheel mechanism discussion, the details of this study will be discussed in a later section. In 2015, Wang et al. reported Na_3OX (X = Cl, Br, I).[12] Both Na_3OCl and Na_3OBr are cubic structures at room temperature. Na_3OBr shows a higher ionic conductivity compared to Na_3OCl, though the activation energy of Na_3OBr (0.76 eV) is higher than that of Na_3OCl (0.63 eV). Moreover, halide mixing with iodine to form $Na_3OBr_{0.6}I_{0.4}$ shows a higher ionic conductivity and smaller activation energy (0.63 eV) compared to Na_3OBr, possibly originating from a larger free space or softer anion framework for the Na^+ ion to hop. Sr^{2+} doping also enhances the ionic conductivity by introducing more Na vacancies. The final optimized total ionic conductivity of $Na_{2.9}Sr_{0.05}OBr_{0.6}I_{0.4}$ is 1.9 × 10^{-3} S cm^{-1} at 200 °C. Nguyen et al. investigated Na_3OBr samples prepared through cold-pressing (CP) and spark plasma sintering (SPS).[39] According to the scanning electron microscopy (SEM) results, the area percentage of the porosity was calculated to be 3.98% for the SPS sample and 13.79% for the CP sample. SPS preparation increases the total conductivity of the sample by 1 or 2 orders of magnitude, but the bulk ionic conductivity is still too low for battery applications at 9.02 × 10^{-7} S cm^{-1} at 180 °C.

Theoretical calculations have shown replacing simple halides with an anionic cluster (BH_4^-, BF_4^-, BF_4^-, etc.) greatly enhances the ionic conductivity of antiperovskite electrolytes.[3,40,41] However, as previously discussed, the high ionic conductivity of Na_3OBH_4 still needs further research to confirm.

3.4. K-Ion Conductors

There are fewer studies on K-ion solid state electrolytes compared with Li-ion and Na-ion. Nevertheless, in 2017, Sadikin et al. synthesized $K_3(BH_4)(B_{12}H_{12})$ and studied how both BH_4 and $B_{12}H_{12}$ anion disorder affect the cation mobility.[42] $K_3(BH_4)(B_{12}H_{12})$ has a monoclinic to rhombohedral phase transition at 550 K and a rhombohedral to cubic transition at 675 K. Its ionic conductivity is 10^{-6} S cm^{-1} at 100 °C and requires high temperatures near 400 °C to reach 10^{-3} S cm^{-1}. The authors suggest the reorientation of the larger $B_{12}H_{12}^{2-}$ anion is activated at high temperatures and promotes K-ion mobility, while the disorder of the smaller BH_4^- has no obvious effect. More recently, our group reported K-ion antiperovskite K_3OI.[43] It has a solid–solid phase transition at approximately 240 °C, which induces an increase in ionic conductivity by 2 orders of magnitude. Ba-doped K_3OI–$K_{2.9}Ba_{0.05}OI$ achieved 3.5 × 10^{-3} S cm^{-2} after the phase transition with a low activation energy of 0.36 eV. An advantage of K_3OI compared with other K-ion electrolytes is its intrinsic reduction stability toward K metal. The $K/K_{2.9}Ba_{0.05}OI/K$ symmetric cell shows a low overpotential of 50 mV at 0.5 mA cm^{-2} at 270 °C.

https://doi.org/10.1021/acsmaterialsau.1c00026
ACS Mater. Au 2021, 1, 92–106

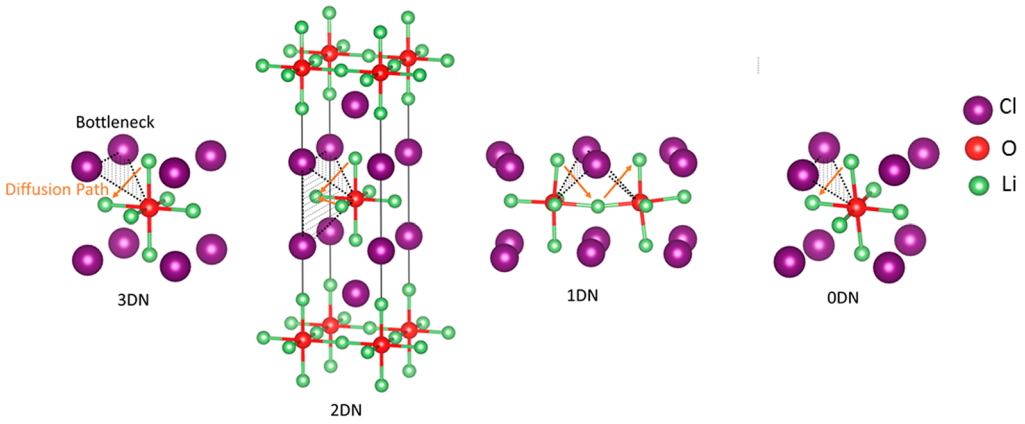

Figure 4. Schematic illustrating the Li diffusion in antiperovskites through the Cl−O−Cl triangular bottleneck. Reproduced with permission from ref 59. Copyright 2020 Elsevier.

4. ION CONDUCTION MECHANISMS

4.1. Three-Dimensional Antiperovskites

The current investigations of the ion transport mechanisms in antiperovskites have primarily relied on theoretical simulations. Before we discuss some of the details, we need to be aware that recent research has pointed out that the claimed "Li_3OCl" can in fact be variants of $Li_2(OH)Cl$ with different hydrogen content.[27] However, as shown below, the current modeling efforts have used the hydrogen-free antiperovskite structure. Therefore, when we examine the modeling results, the difference between the models and the real materials should be noted.

The first question of the ion conduction mechanism is which kind of defect (vacancy or interstitial) is the charge carrier in antiperovskite electrolytes. Based on density functional theory (DFT) calculations, Zhang et al. found that antiperovskites such as Li_3OCl, Li_3OBr, and their mixed compounds are thermodynamically metastable. They identified mobile Li^+ vacancies and anion disorder as the primary driving mechanism for superior ionic conductivities.[25] Li^+ vacancies allow the direct Li hopping along the edge of Li_6O octahedra through a three-coordinate triangular bottleneck site surrounded by the neighboring one oxide and two halide ions with low activation energies (Figure 3a). Their molecular dynamic simulations also reveal partial melting of Li^+ sublattice at about 20 K for Li_3OCl and 50 K for Li_3OBr below the melting point of 500 K. Although the above calculation shows a low barrier, it is still too high to explain superionic conduction.

On the contrary, Emly et al. investigated Frenkel defects and introduced a different kind of defect called an interstitial dumbbell that forms between a Li interstitial and a Li at the Li_6O octahedron (Figure 3b).[24] The migration barrier was calculated to be only 145−175 meV. However, the Frenkel formation energy is as large as 1.94 eV, suggesting only a low concentration of the interstitial dumbbells can be thermally generated.

In 2014, Mouta et al. employed classical atomistic quasi-static calculations to calculate the concentration of Li vacancies and interstitials in Li_3OCl.[51] Vacancies created by Schottky defects were predicted to be the charge carriers in Li_3OCl, as the concentration of interstitials (i.e., Frenkel defects) was 6 orders of magnitude lower due to the very high energy required for their formation. However, in LiCl-deficient materials, the opposite was proposed to be probable due to charge-compensating mechanisms. The defect formation energy of the Schottky Li^+−Cl^- vacancy pair was calculated to be 0.93[25] or 1.27 eV,[52] which are too high to have a high concentration of the charge carrier for Li-ion diffusion. One possibility for forming Li vacancies or interstitials is through deviating from the ideal antiperovskite stoichiometry (1:1 Li_2O/LiCl): LiCl-rich may cause Cl^- to occupy O^{2-} site and increase Li^+ vacancies, while Li_2O-rich may cause O^{2-} to occupy Cl^- sites and increase Li^+ interstitials.

In 2015, Lu et al. employed DFT calculations and classical MD simulations in Li_3OCl to compare LiCl Schottky defects, Li_2O Schottky defects, and Li interstitials charge balanced with O substitution on Cl site.[53] Of the three, LiCl Schottky defects have the lowest binding energy and results in the highest diffusion coefficients. The study indicates Li^+ vacancies are the dominant charge carriers.

Moreover, Stegmaier et al. investigated the defects in Li-ion solid-state batteries.[54] They found that Li^+ interstitials are the dominant species at the anode while Li^+ vacancies dominate at the cathode. With Mg aliovalent doping, Li^+ vacancies are the dominant charge carriers in the bulk of the electrolyte.

Theoretical studies have proposed several approaches to enhance the ionic conduction in antiperovskite electrolytes. Ong et al. have carried out an analysis of the phase stability and ionic conduction mechanisms in $Li_3OCl_{1-n}Br_n$ using a combination of first-principles calculations and percolation theory.[55] A key outcome is the effect of the halide local environment on vacancy migration barriers: when Li^+ hops along the edge of the Li_6O octahedron through a three-coordinate triangular intermediate site, a low migration barrier is achieved when the initial and final sites are Br^--rich and the intermediate triangular site is surrounded by Cl^-. Percolation of such low barrier paths can enhance the ionic conductivity, which provides a strategy to optimize the halide composition. For Li_2OHCl, Ciucci et al. reported that partially replacing Cl^- with F^- also enhances the ionic conductivity.[29] According to the density functional theory result, $Li_2OHF_{0.1}Cl_{0.9}$ has concurrent events and conductivity higher than that of Li_2OHCl and $Li_2OH_{0.9}F_{0.1}Cl$. They also reported that the mismatch of the ions' sizes between F, OH, and Cl induces distortions that widen the Li diffusion channels near F atoms.

Islam et al. investigate the impact of divalent cation (Mg^{2+},Ca^{2+},Sr^{2+}, and Ba^{2+}) and F^- doping on the ion conduction properties of Li_3OCl, using both defect simulation and molecular dynamics techniques.[56] Among all dopants, Mg dopants have the lowest binding energies to lithium vacancies, yielding the highest lithium-ion conductivities and lowest

https://doi.org/10.1021/acsmaterialsau.1c00026
ACS Mater. Au 2021, 1, 92−106

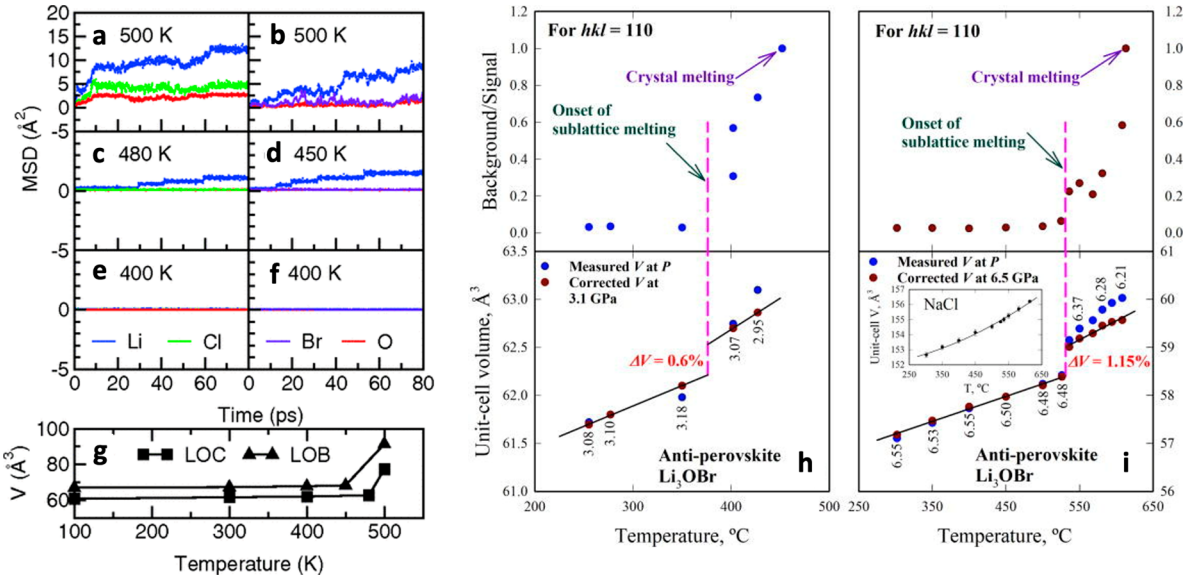

Figure 5. Calculated MSDs of all ion species for Li_3OCl (LOC) and Li_3OBr (LOB) at different stages: (a,b) melting, (c,d) sublattice melting, and (e,f) nonmelting. (g) Volume changes of LOC and LOB as functions of temperature. Reproduced with permission from ref 25. Copyright 2013 American Physical Society. Thermal expansion of antiperovskite Li_3OBr and the corresponding variation of the background/signal ratios as a function of temperature at 3.1 GPa (h) and 6.5 GPa (i). Reproduced with permission from ref 61. Copyright 2020 AIP Publishing.

migration energies. Moreover, their results indicate the binding energies decrease with increased dopant concentration.

Theoretical studies also have been applied to study the grain boundary effects on ionic transport. Dawson et al. employed large-scale molecular dynamics simulations at Li_3OCl.[57] Their results showed that the Li-ion migration through the grain boundaries is hindered as the activation energies for grain boundaries are higher than for the grain. A combination of first principle and phase field calculations from Shen et al. suggests that the defect may segregate at the grain boundary, which lowers the total ionic conductivity of polycrystalline Li_3OCl.[58]

4.2. Low-Dimensional Antiperovskites

In addition to three-dimensional cubic phase antiperovskites, two-dimensional Ruddlesden−Popper (RP) phase antiperovskites, which result from the intergrowth of antiperovskite-layer and rocksalt-layer structures, have been reported as ion conductors. Ciucci et al. used Li−O−Cl as the model system and suggested reducing the dimensionality of antiperovskites as an approach to lower the cation migration barrier energies and improve the cation diffusion coefficients (Figure 4).[59] They pointed out that the lower-dimensional antiperovskites provide larger Cl−O−Cl and Cl−Cl−Cl triangle bottleneck sizes and softer, more flexible lattices. Both factors help Li^+ migration. This is an interesting point that seems to be supported by Zhu's experimental results of RP phase $Li_7O_2Br_3$.[11] They used quenching to synthesize a composite of 44:56 $Li_7O_2Br_3$/Li_3OBr due to the metastable nature of $Li_7O_2Br_3$, with the ionic conductivity reaching 2.4×10^{-5} S cm^{-1} at room temperature, more than 1 order of magnitude higher than the pure phase Li_3OBr compound. However, when Koedtruad et al. synthesized RP phase $LiBr(Li_2OHBr)_2$ and compared its ionic conductivity with the three-dimensional Li_2OHBr, the obtained conductivity of $LiBr(Li_2OHBr)_2$ at 30 °C is 1.27×10^{-7} S cm^{-1} and comparable to that of the cubic phase Li_2OHBr (1.33×10^{-7} S cm^{-1}).[21] The measured activation energy of $LiBr(Li_2OHBr)_2$ is 0.57 eV and is also similar to that of Li_2OHBr (0.55 eV). One possible reason is that the Li-ion conductivity was measured in a polycrystalline sample. The actual (intrinsically two-dimensional) ionic conductivity within the antiperovskite layers in the RP phase may be much larger than that measured here.

Zhu et al. investigated Na_4OI_2 and used in situ neutron diffraction to study the Na^+ ion transport mechanism.[49] The measured ionic conductivity and activation energy are similar to Na_3OBr. Na_4OI_2 has an RP structure that is built from slabs consisting of a single layer of corner-sharing $[ONa_{4/2+2}]$ octahedra. A notable difference from the three-dimensional cubic antiperovskite is that RP contains two symmetrically distinct Na^+ sites: the corner-sharing sites and the unshared apical sites. This introduces more complex ion migration pathways that involve both intralayer and interlayer migrations. Zhu's modeling shows that the sodium migration can be considered mainly inside the "Na_3OI" layer and has an anisotropic transport feature. This makes sense because the interlayer structure can be described as rocksalt, which is not known to support superionic conduction. A recent theoretical investigation by Zhao et al. has considered migration mechanisms of not only different vacancies but also interstitial sites.[60]

4.3. Cation Sublattice Melting

After the first reported superionic behavior of Li_3OCl and $Li_3O(Cl_{0.5}Br_{0.5})$ by Zhao et al.,[1] Zhang et al. observed Li sublattice melting in the AIMD simulation.[25] From the simulation results, Li_3OCl and Li_3OBr follow a linear thermal expansion before 500 K, and both melt at 500 K. From Figure 5c,d, Li shows a large mean square displacement (MSD) while anions remain immobile. The simulated Li sublattice melting temperatures for Li_3OCl and Li_3OBr are 480 and 450 K, respectively. Below the sublattice melting temperatures, the MSD of Li is small, which supports the mechanism that the sublattice melting governs Li^+ migration. Additional MSD calculations for sublattice melting phase at different temperatures would provide better support to Zhao et al.'s conclusion.

Zhang et al. studied the structural disorder and sublattice melting of Li_3OBr up to 6.5 GPa using in situ synchrotron X-ray

https://doi.org/10.1021/acsmaterialsau.1c00026
ACS Mater. Au 2021, 1, 92−106

diffraction.[61] The Li_3OBr sample in that study was synthesized via the dehydration reaction of $Li_5Br(OH)_4 = Li_3OBr + 2LiOH + 2H_2O$. Since $Li_2(OH)Br$ and Li_3OBr have similar lattice parameters and are hard to differentiate by XRD, the interference of the hydroxide group cannot be excluded from the synthesized Li_3OBr. The results in Figure 5h,i show a sudden volume increase when heating from 350 to 400 °C at 3.1 GPa and from 525 to 535 °C at 6.5 GPa. The increased background to signal ratios indicate stronger background scattering, which may reflect Li sublattice melting.

4.4. Paddlewheel Effect: An Explanation for Complex Anion Superionic Behavior

"Paddlewheel" effect has been claimed in several superionic electrolytes, including borohydride (e.g., $NaCB_9H_{10}$),[62] 75 Li_2S–25P_2S_5 glass,[63] and β-Li_3PS_4.[64] It states that higher than expected ionic conductivity can be achieved by correlated motion between a conductive cation and a rotating cluster anion. The term was popularized by Jansen back in 1991, who observed that $Na_3O(NO_2)$ undergoes two conductivity jumps near 500 K whereas Na_3OCN and Na_3OBr undergo only one (Figure 6).[37,38] The jumps in $Na_3O(NO_2)$ and Na_3OCN were larger than the jump in Na_3OBr, which cannot have a rotational component.[37] While Jansen attributed the jump in Na_3OBr to partial melting of the Na sublattice, he argued that the magnitude of the $Na_3O(NO_2)$ and Na_3OCN jumps suggested a combination of sublattice melting and a rotational paddlewheel effect.[37] The presence of an extra conductivity jump in $Na_3O(NO_2)$ could be explained by activating the extra rotational degree of freedom in NO_2^- compared to CN^-.[37,38] Gao et al. confirmed in 2020 that Na_3ONO_2 has a significant conductivity jump at 485 K, and their DFT calculations showed a cooperative mechanism in which an O ion in the NO_2^- cluster first pulls Na^+ out of its equilibrium position and then pushes it into a nearby vacancy, in accordance with a paddlewheel mechanism.[50]

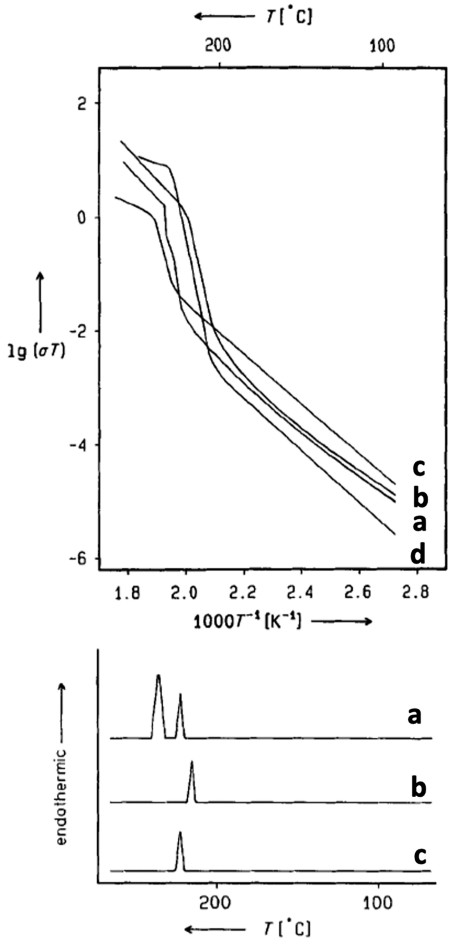

Figure 6. (Top) Sodium ion conductivity in (a) $Na_3O(NO_2)$, (b) $Na_3O(CN)$, (c) $Na_3OBr(c)$, and (d) $Na_4O(NO_2)_2$. (Bottom) Schematic reproduction of the DTA curves of (a–c). Reproduced with permission from ref 37. Copyright 1991 John Wiley and Sons.

In recent years, research into antiperovskites containing cluster anions, such as OH^- in Li_2OHX (X = Cl, Br) and BX_4^- (X = H, F, Cl) in Li_3OBX_4, has increased as impressive ionic conductivities have been reported. Theoretical and experimental investigations into Li_2OHCl have provided solid evidence of a conductivity jump related to a paddlewheel mechanism. Li_2OHCl is stable in the orthorhombic phase at room temperature and transitions to the cubic phase at 38 °C.[18,23,26,44] The phase transition is accompanied by an increase in ionic conductivity from 1.2×10^{-8} S cm^{-1} at 37 °C to 1.4×10^{-6}S cm^{-1} at 39 °C.[44] Above the transition, its ionic conductivity is similar to Li_2OHBr, which is cubic at all temperatures.[36,47] Eilbracht et al. establish with neutron powder diffraction of Li_2ODCl that OD is static in the low-temperature orthorhombic phase but can point to different octahedral faces in the cubic phase.[23] In an impressive experimental study, Song et al. study the conductivities of $Li_{2+n}OH_{1-n}Cl$ materials and reported an order of magnitude increase from 10^{-7} to 2×10^{-6} S cm^{-1} at 40 °C when moving from $Li_{2.7}OH_{0.3}Cl$ to Li_2OHCl.[18] Moving from $Li_{2.7}OH_{0.3}Cl$ to Li_2OHCl increases the Li vacancies 3-fold, and a conductivity increase on that level may be expected as Li vacancies increase. However, the conductivity changes by an order of magnitude and suggests a second effect is present.[18] ^7Li and ^1H MAS NMR by Dawson et al. and Schwering et al. revealed that the Li and H peaks both dramatically narrow between 30 and 40 °C and continue to narrow as the temperature increases.[22,26] This change indicates increased Li and proton motion.[22,26] However, Dawson et al. also reported with MAS NMR that in deuterated Li_2ODCl, D atom rotation does not begin until 69 °C, which is above the transition temperature and implies that the phase transition may not completely coincide with OH/OD motion.[26]

Several DFT studies have corroborated experimental trends and offered mechanisms of Li conduction. Wang et al., Dawson et al., and Howard et al. have shown that the OH clusters are static and confined to the *ac* plane in the orthorhombic phase of Li_2OHCl.[26,44,45] In the cubic phase, the H atoms rotate around O in all three dimensions and move between eight locations, as indicated by AIMD and MEM studies.[26,44] MSD studies with AIMD have confirmed that despite the mobility of the H atom, Li is the conductive ion as H remains confined within 2 Å of the oxygen atom, and Li rapidly moves through the material.[26,44] For the mechanism of Li conductivity, Song et al. completed Born–Oppenheimer molecular dynamics simulations of $Li_{2.92}OH_{0.08}Cl$ and observed concerted motion between three Li and two H atoms in which H rotates away from a vacancy and Li fills the vacancy (Figure 7).[18] The Li movement creates a new vacancy toward which another H atom rotates, opening space for another Li atom to move, and so on.[18] Dawson et al. similarly argue that the H atom prefers to point toward a Li vacancy to lower electrostatic repulsion.[26] When a Li-ion moves to occupy that vacancy, the H atom rotates to point to the new vacancy.

https://doi.org/10.1021/acsmaterialsau.1c00026
ACS Mater. Au 2021, 1, 92–106

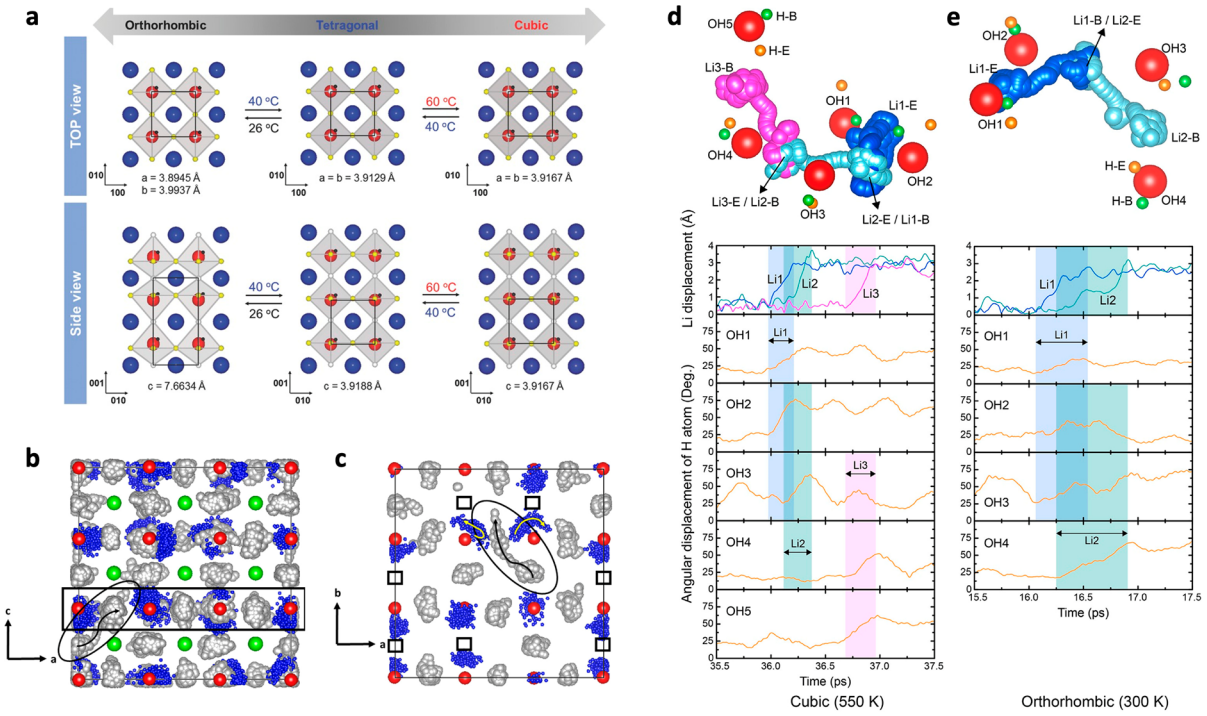

Figure 7. Proposed paddlewheel effect in Li_2OHCl. (a) represents the schematics of the phase transformation of Li_2OHCl. Reproduced with permission from ref 18. Copyright 2017 John Wiley and Sons. (b) Molecular dynamics simulation of Li_2OHCl at T = 640 K. Reproduced with permission from ref 45. Copyright 2017 American Physical Society. (c) Concerted migration of Li^+ in (d) cubic Li_2OHCl at 550 K and (e) orthorhombic Li_2OHCl at 300 K. Reproduced from ref 44. Copyright 2020 American Chemical Society.

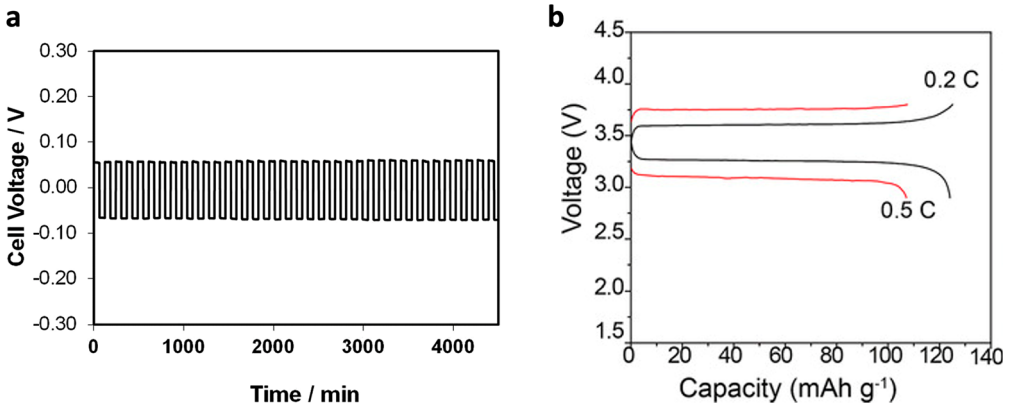

Figure 8. (a) Molten lithium cyclability in a symmetric Li/Li_2OHCl/Li cell with a current density of 1.0 mA cm^{-2} at 195 °C, demonstrating stability between the molten lithium anode and the crystalline electrolyte. Reproduced from ref 30. Copyright 2016 American Chemical Society. (b) Charge and discharge voltage profiles of Li/cross-linked poly(ethylene oxide) (CPEO)−LiTFSI/$Li_2(OH)_{0.9}F_{0.1}Cl$/$LiFePO_4$ all-solid-state battery at 65 °C. Reproduced with permission from ref 28. Copyright 2016 John Wiley and Sons.

The rotation is easier at higher temperatures, so conductivity increases.[26] Wang et al. extended this cooperativity to suggest a paddlewheel mechanism in which three Li atoms and five H atoms move together.[44] Howard et al. reported that the H atoms rotate away from the Li atom as it moves toward a vacancy.[45] This places more initiative on Li movement but is similar to the rest of the simulations. It is difficult to experimentally determine which mechanism is most accurate, and indeed the reality may be a combination of several pathways. Nevertheless, DFT simulations have provided good evidence that a paddlewheel-type mechanism influences the conductivity jump between the orthorhombic and cubic phase transitions of Li_2OHCl.

Investigations of the paddlewheel mechanism in BX_4^- (X = H, F, Cl) cluster ions have had mixed results. Sun et al. synthesized Na_3OBH_4 from Na_2O and $NaBH_4$ using ball milling.[3] They reported an increase in ionic conductivity from 10^{-6} to 10^{-7} S cm^{-1} in Na_3OX (X = Cl, Br, I) to 4.4×10^{-3} S cm^{-1} in Na_3OBH_4 at room temperature. Their CI-NEB calculations connect this to BH_4^- rotation as fixed BH_4^- raises the activation energy of Na^+ conduction from 0.39 to 0.55 eV. Their AIMD calculations with a 2 × 2 × 2 supercell also show Na transport in Na_3OBH_4 faster than that in Na_3OBr.[3] However, Sun et al. could only achieve the high ionic conductivity by hot-pressing at 100 °C. On the contrary, Ahiavi et al. reported an ionic conductivity on the order of 10^{-8} S cm^{-1} at 25 °C for Na_3OBH_4, in line with other Na_3OX materials.[3,12,34] Furthermore, Ahiavi et al. ran AIMD simulations with a larger 3 × 3 × 3 supercell and found Na_3OBr to have faster ionic conductivity compared to Na_3OBH_4.[34]

https://doi.org/10.1021/acsmaterialsau.1c00026
ACS Mater. Au 2021, 1, 92−106

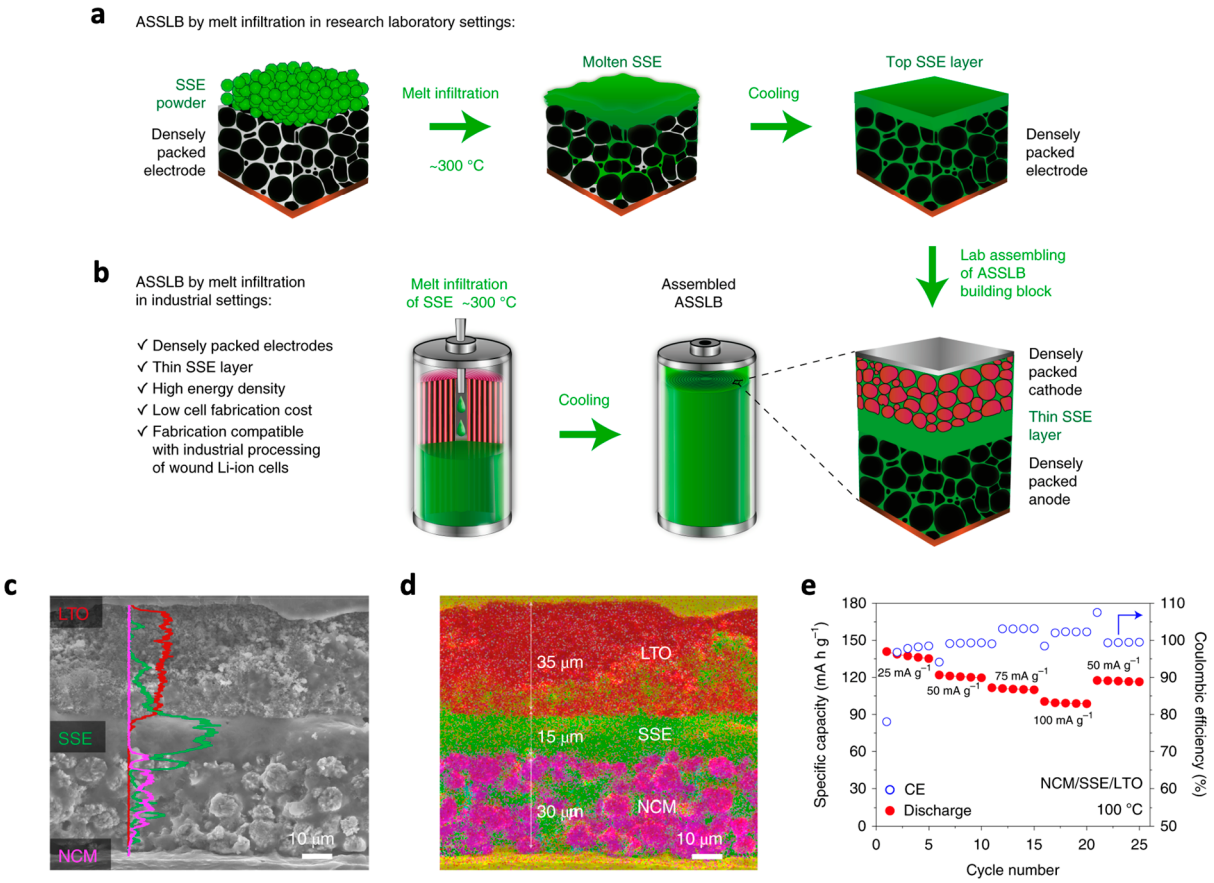

Figure 9. (a) Illustration of melt infiltration in research laboratory settings. (b) Proposed application of melt infiltration in industrial settings (future work). (c) SEM image of an ASSLB cell with an NCM^{111} cathode and LTO anode prepared by the melt-infiltration technique; vertical EDS line scans show Ni (NCM^{111}, purple), Cl (SSE, green) and Ti (LTO, red). (d) EDS mapping of the cross-section of the ASSLB cell, where the purple color represents combined Ni/Co/Mn (NCM^{111}), the red color represents combined Ti/O (LTO) and the green color represents Cl (SSE). (e) Cells cycled at 100 °C in the potential window of 1.0−2.7 V. Reproduced with permission from ref 66. Copyright 2021 Springer Nature.

These results do not disallow the presence of BH_4 rotation but suggest that it is a minor effect.

Fang et al. have reported a series of remarkable conductivities from DFT and AIMD simulations, including 10^{-2} S cm^{-1} for $Li_3S(BF_4)$, 0.1 S cm^{-1} for $Li_3S(BF_4)_{0.5}Cl_{0.5}$, 2.8×10^{-3} S cm^{-1} for $Na_3S(BCl_4)$, and 3.8×10^{-3} S cm^{-1} for $Na_3S(BCl_4)_{0.5}I_{0.5}$, all at room temperature and with activation energies below 0.21 eV.[40,41] MSD data show that preventing BCl_4^- rotation suppresses Na conduction. They argue that combining large anionic clusters with small anions (or vice versa) creates large unit cells with more space for conduction pathways.[41] However, the synthesis and experimental ionic conductivity data of these materials have not been reported.

5. ELECTROCHEMICAL PERFORMANCE AND APPLICATIONS IN BATTERIES

5.1. Antiperovskites as Electrolytes

In 2016, Hood et al. reported that continuous, dense Li_2OHCl membranes could be fabricated at a temperature below 400 °C.[30] The Li_2OHCl solid electrolyte enables molten Li plating/stripping in a Li metal symmetric Li/Li_2OHCl/Li cell with a current density of 1.0 mA cm^{-2} at 195 °C (Figure 8a). It needs to be noted that such a high temperature (195 °C) is not desirable for commercial application, and Li metal is molten at that temperature. According to the EDS results, at the electrolyte/electrode interface, Li_2O was formed and helped stabilize the electrolyte-electrode interface. Li et al. reported F-doped Li_2OHCl−$Li_2(OH)_{0.9}F_{0.1}Cl$ for an all-solid-state-battery at 65 °C.[28] The substitution of F^- for OH^- not only reduces the number of hindering OH^- by smaller size F^- but also stabilizes the cubic phase at room temperature. The all-solid-state Li/cross-linked poly(ethylene oxide) (CPEO)−LiTFSI/$Li_2(OH)_{0.9}F_{0.1}Cl$/$LiFePO_4$ 2032 coin cell shows stable cycling at 0.2 and 0.5 C with high Coulombic efficiency (Figure 8b). It needs to be noted that a Li^+-conducting polymer membrane (CPEO-LiTFSI) was used to reduce the interfacial resistance. Sugumar et al. further showed Li/Li_2OHBr/Li symmetric cell plated/stripped lithium at a current density of 50 μA cm^{-2} with an overpotential of 0.22 V.[47] They claimed that the overpotential mostly originates from the electrolyte resistance. Yoshikawa et al. measured the electrochemical window of Li_2OHBr based on the CV result of Li/Li2OHBr/Au cell.[65] During the first cycle, the irreversible anodic current was observed above 3.5 V, and the irreversible cathodic current peak showed at approximately 1.7 V. The Li/Li_2OHBr/$Fe_2(MoO_4)_3$ all-solid-state batteries fabricated by cold-press showed good cycling stability for 60 cycles. It should be noted that a tiny small current density of 1.0 μA/cm^2 and thin $Fe_2(MoO_4)_3$ layer of 230 nm were used in this all-solid-state battery. In conclusion, Li_2OHX (X = Cl, Br) shows good stability with Li metal anode, likely due to the formation of interfacial Li_2O.

Recently, utilizing the low melting point of Li_2OHCl, Xiao et al. report an electrolyte melt infiltration for scalable manufactur-

https://doi.org/10.1021/acsmaterialsau.1c00026
ACS Mater. Au 2021, 1, 92−106

ing of inorganic all-solid-state batteries (Figure 9).[66] During the fabrication process, liquid Li_2OHCl was infiltrated into electrodes at elevated temperature, which solidify during cooling. The final all-solid-state CR2032 coin cell with $LiNi_{0.33}Mn_{0.33}Co_{0.33}O_2$ cathodes (~1−3.5 mg cm^{-2} mass load) and both $Li_4Ti_5O_{12}$ and graphite anodes show stable cycling at 60 and 100 °C.

5.2. Antiperovskites as Lithium Reservoir and Cathodes

Zhou et al. found that Li_2OHCl can not only be a Li-ion conductor but also a lithium reservoir that can be electrolyzed at 3.3 and/or 4.0 V via two different oxidizing decomposition routes, with the release of Li^+ and the generation of O_2 and HCl.[67] Utilizing the large lithium storage capacity of 810 mAh g^{-1}, Li_2OHCl can be used as a lithium reservoir for Si@C anode prelithiation.

Due to the three-dimensional ion conduction, the antiperovskite structure is a good candidate for cathodes with fast charging ability. Lai et al. reported antiperovskite structure $(Li_2Fe)ChO$ (Ch = S, Se, Te) as Li-ion cathode material.[68] $(Li_2Fe)SO$ and $(Li_2Fe)SeO$ show cubic structure and $(Li_2Fe)TeO$ shows hexagonal structure (Figure 10a,b). $(Li_2Fe)SeO$

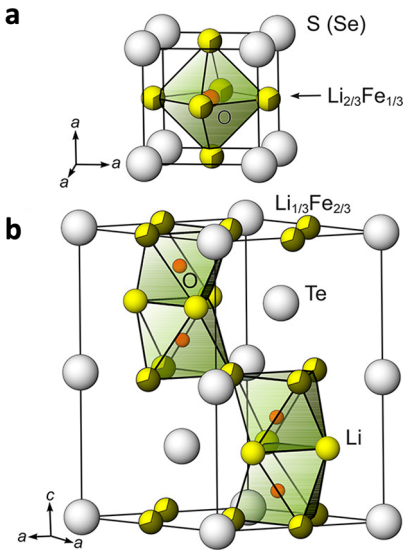

Figure 10. Crystal structures of $(Li_2Fe)ChO$ (Ch = S, Se, Te). (a) Cubic antiperovskites $(Li_2Fe)ChO$ (Ch = S, Se) and (b) 4H-hexagonal antiperovskite $(Li_2Fe)TeO$. Reproduced from ref 68. Copyright 2017 American Chemical Society.

exhibits charge capacities of approximately 120 mAh g^{-1} at a charge rate of 30 mA g^{-1}. Later an operando study on $(Li_2Fe)SO$ reveals that Fe is the main redox center at a low charging current and S is involved at higher charging currents.[69] It is also shown that Fe substitution (even only 10%) in Li_2FeSO by Co or Mn significantly changes the structural behavior during battery cycling. The Co substitution improves the cyclability, whereas Mn substitution deteriorates the cycling performance.[70,71] Theoretical study shows the Li-ion diffusion barrier in $(Li_2Fe)SO$ is only 0.32 eV, which may explain its good rate capacity.[72] $Li_2Fe_2S_2O$ and $Li_4Fe_3S_3O_2$ with anti-RP structure are predicted to have similar voltage as $(Li_2Fe)SO$ and fast Li conduction channels.[73]

For the Na-ion, although Na-containing analogues $(Li_{2-n}Na_nFe)SO$ cannot be synthesized through solid-state reaction, $Na_2Fe_2OS_2$ with anti-RP structure can be synthesized through solid-state or mechanochemical synthesis.[74]

6. CONCLUSION

In this critical review, we detail the crystal structures, compositions, ionic conductivities, and electrochemical applications of antiperovskite electrolytes. Although the impressively high ionic conductivities of $Li_3OCl_{0.5}Br_{0.5}$, Na_3OBH_4, and $Li_{3-2x}Ba_xOCl$ glass (x = 0.005) electrolytes have stimulated intense interests, these materials were not thoroughly characterized, and the reported ionic conductivities have not been independently verified. We would like to recommend some practices for the community to consider in future research reports, especially when stellar, record-breaking ionic conductivities are reported:

(1) Independent verification/certification of ionic conductivities. This practice has been adopted in the photovoltaics community. When people report record-breaking energy conversion efficiencies, they obtain certified measurement results from independent agencies such as the National Renewable Energy Lab (NREL). If a similar practice can be enforced in reporting ionic conductors, questionable results can be avoided.

(2) Attention to details of sample handling. Li and Na salts are often hygroscopic. When they are handled under ambient conditions, absorbing moisture can significantly change their properties. Even when stored and handled in a glovebox, residues of organic vapors in the glovebox can still be absorbed. Elemental analysis after conductivity testing helps verify the purity of the samples.

(3) Repeating ionic conductivity tests with multiple pellet samples and providing statistical analysis. Ideally, at least three pellets with different thicknesses using powder from three different synthesis batches should be measured independently. For impedance data analysis, the equivalent circuits and all the fitting values, including the fitting error, should be provided. Then the average of the three pellets' ionic conductivities should be reported with standard deviation, instead of the ionic conductivity of one pellet. The testing condition, including but not limited to the pressure and temperature for pellet preparation, the sintering procedure, the material and fabrication of blocking electrode, the testing environment (e.g., in air, inside the glovebox, coin cell, or Swagelok cell), and the stack pressure applied, should be included in the experimental section.

(4) Reporting the testing condition of solid-state batteries. For solid-state batteries, the testing condition affects the final performance significantly. When reporting the solid-state battery data, people should also report the details of the batteries, including the procedure to prepare the batteries, the working temperature, the stack pressure applied, and the active material amount, etc.

If we take out the above three stellar antiperovskites, the highest reported ionic conductivity at room temperature is approximately 10^{-4}−10^{-5} and 10^{-6}−10^{-7} S cm^{-1} for Li-ion antiperovskite electrolytes and Na-ion antiperovskite electrolytes, respectively. Methods like anion mixing, OH substitution, quenching, and multivalent cation doping have been useful strategies to enhance ionic conductivities. Moreover, two-dimensional antiperovskites may have a higher bulk conductivity compared with three-dimensional antiperovskites. The actual

https://doi.org/10.1021/acsmaterialsau.1c00026
ACS Mater. Au 2021, 1, 92−106

ion conduction mechanism is still under debate. Theoretical studies showed Li^+ vacancies have lower formation energies but higher migration barrier energies, while interstitial Li^+ defects have higher formation energies but a lower barrier for migration. Several experimental and theoretical studies stated polyanions (e.g., OH^- or BH_4^-) facilitate cation migration through the paddlewheel mechanism, although the degree by which the paddlewheel mechanism improves ionic conductivity varies widely by material. For battery applications, $Li_2(OH)Cl$ has been shown to have good stability toward Li metal anodes. Most recently, utilizing the low melting point of Li_2OHCl, an electrolyte melt infiltration method for scalable manufacturing of inorganic all-solid-state batteries has been reported.

Using a review on solid-state electrolytes as a reference,[75] the properties of antiperovskites are summarized in a spider plot, as shown in Figure 11. The low ionic conductivities of the

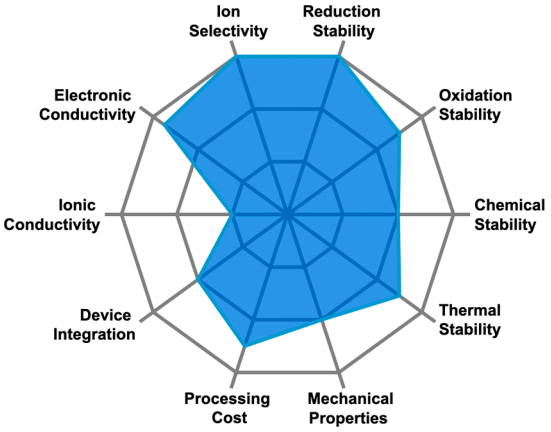

Figure 11. Spider plot of the antiperovskite electrolyte materials. For ionic conductivity, the three stellar antiperovskites ($Li_3OCl_{0.5}Br_{0.5}$, Na_3OBH_4, and $Li_{3-2x}Ba_xOCl$ glass (x = 0.005)), which need further examination are not included. The value of each property for antiperovskite electrolyte is estimated by comparing with reported oxide, sulfide, hydride, halide, thin films, and polymer solid electrolytes.[75]

antiperovskite electrolyte greatly limits their overall performance. However, antiperovskite electrolytes, compared with other solid-state electrolytes, still have several unique advantages. Although oxide- and sulfide-based electrolytes have good mechanical rigidity, they are challenging for device integration. Polymer electrolytes are easier for device fabrication. However, they have weaker mechanical strength and low ion selectivity. Antiperovskite electrolytes including $Li_2(OH)Cl$ have been reported to have easy scalable manufacturing, high ion selectivity, and good mechanical rigidity,[66] comprising the advantages of oxide- and sulfide-based electrolytes and polymer electrolytes. In addition, antiperovskite electrolytes also maintain easy synthesis.

Another important advantage is the intrinsic reduction stability of alkali metal oxyhalide antiperovskite (M_3OX). For example, K_3OI has been shown to have intrinsic reduction stability toward K metal.[43] The $K/K_{2.9}Ba_{0.05}OI/K$ symmetric cell shows a consistent low overpotential of 50 mV at 0.5 mA cm^{-2} at 270 °C. The other commonly used alkali metal solid-state electrolytes, such as $Li_{10}GeP_2S_{12}$ (LGPS), LPS, Na_3PS_4, and even the most cathodic stable $Li_7La_3Zr_2O_{12}$ (LLZO), are not intrinsically stable toward Li or Na metal anodes.[76,77]

Future development of antiperovskite electrolytes should prioritize increasing the room temperature ionic conductivity. More research should be done to examine the three stellar antiperovskites with reported high ionic conductivity ($Li_3OCl_{0.5}Br_{0.5}$, Na_3OBH_4, and $Li_{3-2x}Ba_xOCl$ glass (x = 0.005)). Different doping methods can be tried to increase charge carrier concentration or mobility. It is worth noting that lower-dimensional antiperovskite has been suggested to have a lower migration barrier and high diffusion coefficient compared with cubic antiperovskite. Improving the fabrication, such as modifying the sintering process, making thin films, may also effectively decrease the final area-specific resistance.

AUTHOR INFORMATION

Corresponding Author

Yiying Wu − *Department of Chemistry and Biochemistry, The Ohio State University, Columbus, Ohio 43210, United States;* orcid.org/0000-0001-9359-1863; Email: wu@chemistry.ohio-state.edu

Authors

Jingfeng Zheng − *Department of Chemistry and Biochemistry, The Ohio State University, Columbus, Ohio 43210, United States*

Brian Perry − *Department of Chemistry and Biochemistry, The Ohio State University, Columbus, Ohio 43210, United States*

Complete contact information is available at: https://pubs.acs.org/10.1021/acsmaterialsau.1c00026

Notes

The authors declare no competing financial interest.

ACKNOWLEDGMENTS

This work was financially supported by the Ohio State University and the U.S. Department of Energy (Award No. DE-FG02-07ER46427).

REFERENCES

(1) Zhao, Y.; Daemen, L. L. Superionic Conductivity in Lithium-Rich Anti-Perovskites. *J. Am. Chem. Soc.* **2012**, *134* (36), 15042−15047.

(2) Braga, M. H.; Ferreira, J. A.; Stockhausen, V.; Oliveira, J. E.; El-Azab, A. Novel Li3ClO Based Glasses with Superionic Properties for Lithium Batteries. *J. Mater. Chem. A* **2014**, *2* (15), 5470−5480.

(3) Sun, Y.; Wang, Y.; Liang, X.; Xia, Y.; Peng, L.; Jia, H.; Li, H.; Bai, L.; Feng, J.; Jiang, H.; et al. Rotational Cluster Anion Enabling Superionic Conductivity in Sodium-Rich Antiperovskite Na 3 OBH 4. *J. Am. Chem. Soc.* **2019**, *141* (14), 5640−5644.

(4) Goldschmidt, V. M. Die Gesetze Der Krystallochemie. *Naturwissenschaften* **1926**, *14* (21), 477−485.

(5) Avdontceva, M. S.; Zolotarev, A. A.; Krivovichev, S. V. Order-Disorder Phase Transition in the Antiperovskite-Type Structure of Synthetic Kogarkoite, Na3SO4F. *J. Solid State Chem.* **2015**, *231*, 42−46.

(6) Gao, S.; Broux, T.; Fujii, S.; Tassel, C.; Yamamoto, K.; Xiao, Y.; Oikawa, I.; Takamura, H.; Ubukata, H.; Watanabe, Y.; et al. Hydride-Based Antiperovskites with Soft Anionic Sublattices as Fast Alkali Ionic Conductors. *Nat. Commun.* **2021**, *12* (1), 1−10.

(7) Chiodelli, G.; Magistris, A.; Schiraldi, A. Ag3SBr and Ag3SI: Ionic Conductivity of Their Modifications in the Range 93−573. *Z. Phys. Chem.* **1979**, *118* (2), 177−186.

(8) Yin, L.; Murphy, M.; Kim, K.; Hu, L.; Cabana, J.; Siegel, D. J.; Lapidus, S. H. Synthesis of Antiperovskite Solid Electrolytes: Comparing Li $_3$ SI, Na $_3$ SI, and Ag $_3$ SI. *Inorg. Chem.* **2020**, *59* (16), 11244−11247.

(9) Shannon, R. D. Revised Effective Ionic Radii and Systematic Studies of Interatomic Distances in Halides and Chalcogenides. *Acta Crystallogr., Sect. A: Cryst. Phys., Diffr., Theor. Gen. Crystallogr.* **1976**, *32* (5), 751−767.
(10) Roobottom, H. K.; Jenkins, H. D. B.; Passmore, J.; Glasser, L. Thermochemical Radii of Complex Ions. *J. Chem. Educ.* **1999**, *76* (11), 1570−1572.
(11) Zhu, J.; Li, S.; Zhang, Y.; Howard, J. W.; Lü, X.; Li, Y.; Wang, Y.; Kumar, R. S.; Wang, L.; Zhao, Y. Enhanced Ionic Conductivity with Li7O2Br3 Phase in Li3OBr Anti-Perovskite Solid Electrolyte. *Appl. Phys. Lett.* **2016**, *109* (10), 101904.
(12) Wang, Y.; Wang, Q.; Liu, Z.; Zhou, Z.; Li, S.; Zhu, J.; Zou, R.; Wang, Y.; Lin, J.; Zhao, Y. Structural Manipulation Approaches towards Enhanced Sodium Ionic Conductivity in Na-Rich Antiperovskites. *J. Power Sources* **2015**, *293*, 735−740.
(13) Hippler, K.; Sitta, S.; Vogt, P.; Sabrowsky, H. Kristallstruktur von Na4OBr2/Crystal Structure of Na4OBr2. *Z. Naturforsch., B: J. Chem. Sci.* **1990**, *45* (2), 105−106.
(14) Sabrowsky, H.; Hippler, K.; Sitta, S.; Vogt, P.; Walz, L. Structure of Na4OI2. *Acta Crystallogr., Sect. C: Cryst. Struct. Commun.* **1990**, *46* (3), 368−369.
(15) Jansen, M. Neue Untersuchungen an Na3NO3. *Z. Anorg. Allg. Chem.* **1977**, *435* (1), 13−20.
(16) Müller, W.; Jansen, M. A4N2O5 (A = Na, K), Neue Oxidnitrite Der Alkalimetalle Und Eine Bemerkung Zum Quasi-Binären System K3NO3/K3OBr. *Z. Anorg. Allg. Chem.* **1992**, *610* (4), 28−32.
(17) Hardt, C.; Vogt, P.; Sabrowsky, H. Kristallstruktur von K4O(CN)2. *Z. Naturforsch., B: J. Chem. Sci.* **1992**, *47* (12), 1746−1748.
(18) Song, A. Y.; Xiao, Y.; Turcheniuk, K.; Upadhya, P.; Ramanujapuram, A.; Benson, J.; Magasinski, A.; Olguin, M.; Meda, L.; Borodin, O.; et al. Protons Enhance Conductivities in Lithium Halide Hydroxide/Lithium Oxyhalide Solid Electrolytes by Forming Rotating Hydroxy Groups. *Adv. Energy Mater.* **2018**, *8* (3), 1700971.
(19) Hartwig, P.; Weppner, W. Ionic Conductivities of Lithium-Halide-Based Quaternary Compounds. *Solid State Ionics* **1981**, *3*−*4* (C), 249−254.
(20) Hönnerscheid, A.; Nuss, J.; Mühle, C.; Jansen, M. Die Kristallstrukturen Der Hydroxyhalogenide Li4(OH)3Br Und Li4-(OH)3I. *Z. Anorg. Allg. Chem.* **2003**, *629* (2), 317−320.
(21) Koedtruad, A.; Amano Patino, M.; Chuang, Y. C.; Chen, W. T.; Kan, D.; Shimakawa, Y. Ruddlesden-Popper Phases of Lithium-Hydroxide-Halide Antiperovskites: Two Dimensional Li-Ion Conductors. *RSC Adv.* **2020**, *10* (68), 41816−41820.
(22) Schwering, G.; Hönnerscheid, A.; Van Wüllen, L.; Jansen, M. High Lithium Ionic Conductivity in the Lithium Halide Hydrates Li3-n(OHn)Cl ($0.83 \leq n \leq 2$) and Li3-n(OHn)Br ($1 \leq n \leq 2$) at Ambient Temperatures. *ChemPhysChem* **2003**, *4* (4), 343−348.
(23) Eilbracht, C.; Kockelmann, W.; Hohlwein, D.; Jacobs, H. Orientational Disorder in Perovskite like Structures of Li2X(OD) (X═ Cl, Br) and LiBr · D2O. *Phys. B* **1997**, *234*−*236*, 48−50.
(24) Emly, A.; Kioupakis, E.; Van der Ven, A. Phase Stability and Transport Mechanisms in Antiperovskite Li 3 OCl and Li 3 OBr Superionic Conductors. *Chem. Mater.* **2013**, *25* (23), 4663−4670.
(25) Zhang, Y.; Zhao, Y.; Chen, C. Ab Initio Study of the Stabilities of and Mechanism of Superionic Transport in Lithium-Rich Antiperovskites. *Phys. Rev. B: Condens. Matter Mater. Phys.* **2013**, *87* (13), 134303.
(26) Dawson, J. A.; Attari, T. S.; Chen, H.; Emge, S. P.; Johnston, K. E.; Islam, M. S. Elucidating Lithium-Ion and Proton Dynamics in Anti-Perovskite Solid Electrolytes. *Energy Environ. Sci.* **2018**, *11* (10), 2993−3002.
(27) Hanghofer, I.; Redhammer, G. J.; Rohde, S.; Hanzu, I.; Senyshyn, A.; Wilkening, H. M. R.; Rettenwander, D. Untangling the Structure and Dynamics of Lithium-Rich Anti-Perovskites Envisaged as Solid Electrolytes for Batteries. *Chem. Mater.* **2018**, *30* (22), 8134−8144.
(28) Li, Y.; Zhou, W.; Xin, S.; Li, S.; Zhu, J.; Lü, X.; Cui, Z.; Jia, Q.; Zhou, J.; Zhao, Y.; et al. Fluorine-Doped Antiperovskite Electrolyte for All-Solid-State Lithium-Ion Batteries. *Angew. Chem., Int. Ed.* **2016**, *55* (34), 9965−9968.
(29) Effat, M. B.; Liu, J.; Lu, Z.; Wan, T. H.; Curcio, A.; Ciucci, F. Stability, Elastic Properties, and the Li Transport Mechanism of the Protonated and Fluorinated Antiperovskite Lithium Conductors. *ACS Appl. Mater. Interfaces* **2020**, *12* (49), 55011−55022.
(30) Hood, Z. D.; Wang, H.; Samuthira Pandian, A.; Keum, J. K.; Liang, C. Li 2 OHCl Crystalline Electrolyte for Stable Metallic Lithium Anodes. *J. Am. Chem. Soc.* **2016**, *138* (6), 1768−1771.
(31) Li, S.; Zhu, J.; Wang, Y.; Howard, J. W.; Lü, X.; Li, Y.; Kumar, R. S.; Wang, L.; Daemen, L. L.; Zhao, Y. Reaction Mechanism Studies towards Effective Fabrication of Lithium-Rich Anti-Perovskites Li3OX (X = Cl, Br). *Solid State Ionics* **2016**, *284*, 14−19.
(32) Funke, K.; Heimann, B.; Vering, M.; Wilmer, D. Concept of Mismatch and Relaxation Explains DC and AC Conductivities of Fragile Glass-Forming Ionic Melts. *J. Electrochem. Soc.* **2001**, *148* (5), A395.
(33) Yim, C.-H.; Abu-Lebdeh, Y. A. Connection between Phase Diagram, Structure and Ion Transport in Liquid, Aqueous Electrolyte Solutions of Lithium Chloride. *J. Electrochem. Soc.* **2018**, *165* (3), A547−A556.
(34) Ahiavi, E.; Dawson, J. A.; Kudu, U.; Courty, M.; Islam, M. S.; Clemens, O.; Masquelier, C.; Famprikis, T. Mechanochemical Synthesis and Ion Transport Properties of Na3OX (X = Cl, Br, I and BH4) Antiperovskite Solid Electrolytes. *J. Power Sources* **2020**, *471*, 228489.
(35) Sugumar, M. K.; Yamamoto, T.; Motoyama, M.; Iriyama, Y. Tailoring the Lithium-Ion Conductivity of Li 2 OHBr by Substitution of Bromine with Other Halogens. *Chem. Lett.* **2021**, *50* (3), 448−451.
(36) Koedtruad, A.; Patino, M. A.; Ichikawa, N.; Kan, D.; Shimakawa, Y. Crystal Structures and Ionic Conductivity in Li2OHX (X = Cl, Br) Antiperovskites. *J. Solid State Chem.* **2020**, *286*, 121263.
(37) Jansen, M. Volume Effect or Paddle-Wheel Mechanism—Fast Alkali-Metal Ionic Conduction in Solids with Rotationally Disordered Complex Anions. *Angew. Chem., Int. Ed. Engl.* **1991**, *30* (12), 1547−1558.
(38) Jansen, M.; Feldmann, C.; Müller, W. Über Die Quasi-binären Systeme NaNO2/Na2O Und NaCN/Na2O. Phasendiagramme Und Natrium-Ionenleitung in Na3O(NO2) Und Na3O(CN). *Z. Anorg. Allg. Chem.* **1992**, *611* (5), 7−10.
(39) Nguyen, H.; Hy, S.; Wu, E.; Deng, Z.; Samiee, M.; Yersak, T.; Luo, J.; Ong, S. P.; Meng, Y. S. Experimental and Computational Evaluation of a Sodium-Rich Anti-Perovskite for Solid State Electrolytes. *J. Electrochem. Soc.* **2016**, *163* (10), A2165−A2171.
(40) Fang, H.; Jena, P. Li-Rich Antiperovskite Superionic Conductors Based on Cluster Ions. *Proc. Natl. Acad. Sci. U. S. A.* **2017**, *114* (42), 11046−11051.
(41) Fang, H.; Jena, P. Sodium Superionic Conductors Based on Clusters. *ACS Appl. Mater. Interfaces* **2019**, *11* (1), 963−972.
(42) Sadikin, Y.; Skoryunov, R. V.; Babanova, O. A.; Soloninin, A. V.; Lodziana, Z.; Brighi, M.; Skripov, A. V.; Černý, R. Anion Disorder in K3BH4B12H12 and Its Effect on Cation Mobility. *J. Phys. Chem. C* **2017**, *121* (10), 5503.
(43) Zheng, J.; Fang, H.; Fan, L.; Ren, Y.; Jena, P.; Wu, Y. Antiperovskite K3OI for K-Ion Solid State Electrolyte. *J. Phys. Chem. Lett.* **2021**, *12*, 7120−7126.
(44) Wang, F.; Evans, H. A.; Kim, K.; Yin, L.; Li, Y.; Tsai, P. C.; Liu, J.; Lapidus, S. H.; Brown, C. M.; Siegel, D. J.; et al. Dynamics of Hydroxyl Anions Promotes Lithium Ion Conduction in Antiperovskite Li2OHCl. *Chem. Mater.* **2020**, *32* (19), 8481−8491.
(45) Howard, J.; Hood, Z. D.; Holzwarth, N. A. W. Fundamental Aspects of the Structural and Electrolyte Properties of Li2OHCl from Simulations and Experiment. *Phys. Rev. Mater.* **2017**, *1* (7), 075406.
(46) Lü, X.; Wu, G.; Howard, J. W.; Chen, A.; Zhao, Y.; Daemen, L. L.; Jia, Q. Li-Rich Anti-Perovskite Li3OCl Films with Enhanced Ionic Conductivity. *Chem. Commun.* **2014**, *50* (78), 11520−11522.
(47) Sugumar, M. K.; Yamamoto, T.; Motoyama, M.; Iriyama, Y. Room Temperature Synthesis of Anti-Perovskite Structured Li2OHBr. *Solid State Ionics* **2020**, *349*, 115298.
(48) Yin, L.; Yuan, H.; Kong, L.; Lu, Z.; Zhao, Y. Engineering Frenkel Defects of Anti-Perovskite Solid-State Electrolytes and Their

https://doi.org/10.1021/acsmaterialsau.1c00026
ACS Mater. Au 2021, 1, 92−106

Applications in All-Solid-State Lithium-Ion Batteries. *Chem. Commun.* **2020**, *56* (8), 1251−1254.
(49) Zhu, J.; Wang, Y.; Li, S.; Howard, J. W.; Neuefeind, J.; Ren, Y.; Wang, H.; Liang, C.; Yang, W.; Zou, R.; et al. Sodium Ion Transport Mechanisms in Antiperovskite Electrolytes Na 3 OBr and Na 4 OI 2: An in Situ Neutron Diffraction Study. *Inorg. Chem.* **2016**, *55* (12), 5993−5998.
(50) Gao, L.; Zhang, H.; Wang, Y.; Li, S.; Zhao, R.; Wang, Y.; Gao, S.; He, L.; Song, H.-F.; Zou, R.; et al. Mechanism of Enhanced Ionic Conductivity by Rotational Nitrite Group in Antiperovskite Na_3ONO_2. *J. Mater. Chem. A* **2020**, *8* (40), 21265−21272.
(51) Mouta, R.; Melo, M. Á. B.; Diniz, E. M.; Paschoal, C. W. A. Concentration of Charge Carriers, Migration, and Stability in Li3OCl Solid Electrolytes. *Chem. Mater.* **2014**, *26* (24), 7137−7144.
(52) Wu, M.; Xu, B.; Lei, X.; Huang, K.; Ouyang, C. Bulk Properties and Transport Mechanisms of a Solid State Antiperovskite Li-Ion Conductor Li3OCl: Insights from First Principles Calculations. *J. Mater. Chem. A* **2018**, *6* (3), 1150−1160.
(53) Lu, Z.; Chen, C.; Baiyee, Z. M.; Chen, X.; Niu, C.; Ciucci, F. Defect Chemistry and Lithium Transport in Li3OCl Anti-Perovskite Superionic Conductors. *Phys. Chem. Chem. Phys.* **2015**, *17* (48), 32547−32555.
(54) Stegmaier, S.; Voss, J.; Reuter, K.; Luntz, A. C. Li + Defects in a Solid-State Li Ion Battery: Theoretical Insights with a Li_3OCl Electrolyte. *Chem. Mater.* **2017**, *29* (10), 4330−4340.
(55) Deng, Z.; Radhakrishnan, B.; Ong, S. P. Rational Composition Optimization of the Lithium-Rich Li 3 OCl 1- x Br x Anti-Perovskite Superionic Conductors. *Chem. Mater.* **2015**, *27* (10), 3749−3755.
(56) Clarke, M. J.; Dawson, J. A.; Mays, T. J.; Islam, M. S. Atomistic Insights into the Effects of Doping and Vacancy Clustering on Li-Ion Conduction in the Li 3 OCl Antiperovskite Solid Electrolyte. *ACS Appl. Energy Mater.* **2021**, *4*, 5094.
(57) Dawson, J. A.; Canepa, P.; Famprikis, T.; Masquelier, C.; Islam, M. S. Atomic-Scale Influence of Grain Boundaries on Li-Ion Conduction in Solid Electrolytes for All-Solid-State Batteries. *J. Am. Chem. Soc.* **2018**, *140* (1), 362−368.
(58) Shen, K.; Wang, Y.; Zhang, J.; Zong, Y.; Li, G.; Zhao, C.; Chen, H. Revealing the Effect of Grain Boundary Segregation on Li Ion Transport in Polycrystalline Anti-Perovskite Li3ClO: A Phase Field Study. *Phys. Chem. Chem. Phys.* **2020**, *22* (5), 3030−3036.
(59) Lu, Z.; Liu, J.; Ciucci, F. Superionic Conduction in Low-Dimensional-Networked Anti-Perovskites. *Energy Storage Mater.* **2020**, *28*, 146−152.
(60) Zhao, S.; Chen, C.; Li, H.; Zhang, W. Theoretical Insights into the Diffusion Mechanism of Alkali Ions in Ruddlesden-Popper Antiperovskites. *New J. Chem.* **2021**, *45* (9), 4219−4226.
(61) Zhang, J.; Wang, L.; Zhu, J.; Zhao, Y. Structural Disorder, Sublattice Melting, and Thermo-Elastic Properties of Anti-Perovskite Li3OBr under High Pressure and Temperature. *Appl. Phys. Lett.* **2020**, *117* (8), 081904.
(62) Tang, W. S.; Matsuo, M.; Wu, H.; Stavila, V.; Zhou, W.; Talin, A. A.; Soloninin, A. V.; Skoryunov, R. V.; Babanova, O. A.; Skripov, A. V.; et al. Liquid-Like Ionic Conduction in Solid Lithium and Sodium Monocarba-Closo-Decaborates Near or at Room Temperature. *Adv. Energy Mater.* **2016**, *6* (8), 1502237.
(63) Smith, J. G.; Siegel, D. J. Low-Temperature Paddlewheel Effect in Glassy Solid Electrolytes. *Nat. Commun.* **2020**, *11* (1), 1−11.
(64) Zhang, Z.; Li, H.; Kaup, K.; Zhou, L.; Roy, P. N.; Nazar, L. F. Targeting Superionic Conductivity by Turning on Anion Rotation at Room Temperature in Fast Ion Conductors. *Matter* **2020**, *2* (6), 1667−1684.
(65) Yoshikawa, K.; Yamamoto, T.; Sugumar, M. K.; Motoyama, M.; Iriyama, Y. Room Temperature Operation and High Cycle Stability of an All-Solid-State Lithium Battery Fabricated by Cold Pressing Using Soft Li2OHBr Solid Electrolyte. *Energy Fuels* **2021**, *35* (15), 12581−12587.
(66) Xiao, Y.; Turcheniuk, K.; Narla, A.; Song, A. Y.; Ren, X.; Magasinski, A.; Jain, A.; Huang, S.; Lee, H.; Yushin, G. Electrolyte Melt Infiltration for Scalable Manufacturing of Inorganic All-Solid-State Lithium-Ion Batteries. *Nat. Mater.* **2021**, *20*, 984−990.
(67) Zhou, W.; Guo, L.; Xin, C.; Gao, J.; Zhu, J.; Hu, Y.; Zhang, Y.; Li, J.; Fan, X.; Li, Y. The Electrolysis of Anti-perovskite Li2OHCl for Prelithiation of High Energy Density Batteries. *Angew. Chem.* **2021**, *133*, 13123.
(68) Lai, K. T.; Antonyshyn, I.; Prots, Y.; Valldor, M. *Anti* -Perovskite Li-Battery Cathode Materials. *J. Am. Chem. Soc.* **2017**, *139* (28), 9645−9649.
(69) Mikhailova, D.; Giebeler, L.; Maletti, S.; Oswald, S.; Sarapulova, A.; Indris, S.; Hu, Z.; Bednarcik, J.; Valldor, M. Operando Studies of Antiperovskite Lithium Battery Cathode Material (Li 2 Fe)SO. *ACS Appl. Energy Mater.* **2018**, *1* (11), 6593−6599.
(70) Gorbunov, M. V.; Carrocci, S.; Maletti, S.; Valldor, M.; Doert, T.; Hampel, S.; Gonzalez Martinez, I. G.; Mikhailova, D.; Gräßler, N. Synthesis of (Li2Fe1-YMny)SO Antiperovskites with Comprehensive Investigations of (Li2Fe0.5Mn0.5)SO as Cathode in Li-Ion Batteries. *Inorg. Chem.* **2020**, *59* (21), 15626−15635.
(71) Gorbunov, M. V.; Carocci, S.; Gonzalez Martinez, I. G.; Baran, V.; Mikhailova, D. Studies of Li2Fe0.9M0.1SO Antiperovskite Materials for Lithium-Ion Batteries: The Role of Partial Fe2+ to M2+ Substitution. *Front. Energy Res.* **2021**, *9*, 110.
(72) Lu, Z.; Ciucci, F. Anti-Perovskite Cathodes for Lithium Batteries. *J. Mater. Chem. A* **2018**, *6* (12), 5185−5192.
(73) Zhu, B.; Scanlon, D. Predicting Stable Lithium Iron Oxysulphides for Battery Cathodes *ChemRxiv* **2021**; https://chemrxiv.org/engage/chemrxiv/article-details/60d0a120afe54f1e3fa45bc7.
(74) Gamon, J.; Perez, A. J.; Jones, L. A. H.; Zanella, M.; Daniels, L. M.; Morris, R. E.; Tang, C. C.; Veal, T. D.; Hardwick, L. J.; Dyer, M. S.; et al. Na2Fe2OS2, a New Earth Abundant Oxysulphide Cathode Material for Na-Ion Batteries. *J. Mater. Chem. A* **2020**, *8* (39), 20553−20569.
(75) Manthiram, A.; Yu, X.; Wang, S. Lithium Battery Chemistries Enabled by Solid-State Electrolytes. *Nat. Rev. Mater.* **2017**, 16103.
(76) Zhu, Y.; He, X.; Mo, Y. Origin of Outstanding Stability in the Lithium Solid Electrolyte Materials: Insights from Thermodynamic Analyses Based on First-Principles Calculations. *ACS Appl. Mater. Interfaces* **2015**, *7* (42), 23685−23693.
(77) Richards, W. D.; Miara, L. J.; Wang, Y.; Kim, J. C.; Ceder, G. Interface Stability in Solid-State Batteries. *Chem. Mater.* **2016**, *28* (1), 266−273.

https://doi.org/10.1021/acsmaterialsau.1c00026
ACS Mater. Au 2021, 1, 92−106